

# Implementation of Remote Sensing and GIS Techniques to Study the Flash Flood Risk at NEOM Mega-City, Saudi Arabia

Ahmed A. Abdulalim<sup>1</sup>, Tarek A. El Damaty<sup>2</sup>

<sup>1</sup>Surveying Master's Degree Program, Civil Engineering Department, Faculty of Engineering and Islamic Architecture, Umm Al-Qura University, Makkah, Saudi Arabia

<sup>2</sup>Civil Engineering Department, Faculty of Engineering and Islamic Architecture, Umm Al-Qura University, Makkah, Saudi Arabia  
Email: s44287321@st.uqu.edu.sa, eng\_aleem@hotmail.com, tadamaty@uqu.edu.sa, tdamaty@hotmail.com

**How to cite this paper:** Abdulalim, A.A. and El Damaty, T.A. (2022) Implementation of Remote Sensing and GIS Techniques to Study the Flash Flood Risk at NEOM Mega-City, Saudi Arabia. *Advances in Remote Sensing*, 11, 121-157.  
<https://doi.org/10.4236/ars.2022.114008>

**Received:** March 21, 2022

**Accepted:** November 25, 2022

**Published:** November 28, 2022

Copyright © 2022 by author(s) and Scientific Research Publishing Inc.

This work is licensed under the Creative Commons Attribution International License (CC BY 4.0).

<http://creativecommons.org/licenses/by/4.0/>



Open Access

## Abstract

Southern Red Sea flooding is common. Assessing flood-prone development risks helps decrease life and property threats. It tries to improve flood awareness and advocate property owner steps to lessen risk. DEMs and topography data were analyzed by RS and GIS. Fifth-through seventh-order rivers were studied. Morphometric analysis assessed the area's flash flood danger. NEOM has 14 catchments. We determined each catchment's area, perimeter, maximum length, total stream length, minimum and maximum elevations. It also uses remote sensing. It classifies Landsat 8 photos for land use and cover maps. Image categorization involves high-quality Landsat satellite images and secondary data, plus user experience and knowledge. This study used the wetness index, elevation, slope, stream power index, topographic roughness index, normalized difference vegetation index, sediment transport index, stream order, flow accumulation, and geological formation. Analytic hierarchy considered all earlier criteria (AHP). The geometric consistency index GCI (0.15) and the consistency ratio CR (4.3%) are calculated. The study showed five degrees of flooding risk for Wadi Zawhi and four for Wadi Surr, from very high to very low. 9.16% of Wadi Surr is vulnerable to very high flooding, 50% to high flooding, 40% to low flooding, and 0.3% to very low flooding. Wadi Zawhi's flood risk is 0.23% high, moderate, low, or extremely low. They're in Wadi Surr and Wadi Zawhi. Flood mapping helps prepare for emergencies. Flood-prone areas should prioritize resilience.

## Keywords

Geographic Information System (GIS), Remote Sensing, Flash Floods Hazard Assessment, Analytic Hierarchy Process (AHP), Morphometric Analysis, Hydrology Analysis

## 1. Introduction

Many regions around the world are frequently affected by water shortages. These occurrences can be very harmful to human communities. Flash floods are natural occurrences with a high occurrence velocity. Recent decades have seen an increase in the frequency and severity of these events due to climate change. At the same time, the extensive annual flood and flash flood damages reveal many regions' high vulnerability to these widespread hazards. Basin morphometric surveys establish evaluation parameters for the hydrological system's behavior in basin areas. Landscape shape is measured quantitatively by morphometry. Landforms are defined by their size, elevation (maximum, minimum, or average), and slope. In addition to comparing landforms objectively, geomorphologists can use quantitative data to identify a region's unique characteristics. Using geomorphology and geology, this study contributes to developing a primary hydrological diagnosis that can be used to forecast basin behavior during heavy rainstorms. IAHS-UNESCOWMO (1974) defines flash floods as sudden, high peak discharge floods caused by severe weather thunderstorms. Since the project is located in a floodplain, flash floods are a major risk. Flash flooding occurs when heavy rainfalls in short bursts, often from severe thunderstorms. It occurs in almost every region of Saudi Arabia and causes the most flooding-related deaths. NEOM drainage basins and watersheds were assessed using GIS and remote sensing techniques. They provide a powerful tool for manipulating and analyzing spatial data. The GIS environment derives and tabulates linear, aerial, and relief parameters. The NEOM region's drainage basins are delineated using DEM data. SRTM 1 Void was used to identify channel initiation nodes from digital raster sources. 90 m spatial resolution. The SRTM helped identify water divide points and then map watersheds. The Arabic word "Wadi" means valley and represents two watercourse-facing terrain bodies (*i.e.*, streams or drainages). A drainage basin includes wadis [1]. There are 14 main Wadi basins with a total area of 13629.6 km<sup>2</sup>, (Wadi Mabrak, Umm Jarfeer, Al Zainah, Haqaf, Efal, Al Nakhlah, Al Batinah, Ayounah, Ad Dubaysa, Ghurr, Sadr, Zawhi, kamrah, and Wadi Surr). These Wadi basins were studied using topographical, geological, and satellite imagery. They are classified as fifth-stream order influence and higher. It was used to classify land use in the study area. This paper also aims to raise planners' awareness of flood geomorphology and the importance of morphometric data in planning. Also, advice for future planning to avoid destructive flood hazards in remote and data-scarce areas is given. The construction of flood prevention structures is recommended to help decision-makers mitigate flash floods (*i.e.*, surface water harvesting systems and artificial groundwater recharge).

## 2. Study Area

The NEOM mega-city project is part of Saudi Arabia's 2030 vision plan to diversify and grow the Saudi economy while positioning the country to lead global development. The Saudi government plans to finish the first section of NEOM

by 2025. NEOM Region is in the upper northwest of Saudi Arabia. It is an intelligent zone with economic, commercial, and tourist destinations. It is located in Tabuk Province (146,072 km<sup>2</sup>), 50 km from Tabuk City, near the Red Sea and Saudi Arabia's borders with Egypt and Jordan. This region will be 26,500 km<sup>2</sup>, with a 225 km Red Sea coastline. So, NEOM Region is located at 27°43'27"N, 29°08'29"N, 34°31'40"E, and 35°57'55"E. NEOM is a prestigious Saudi Arabian project to build a planned mega-city along the northern Red Sea coast (**Figure 1**), bordering Jordan and Egypt. It is a \$500 billion mega-city that will provide world-class healthcare, education, and culture using advanced, automated, zero-carbon infrastructure and forward-thinking, business-friendly governance.

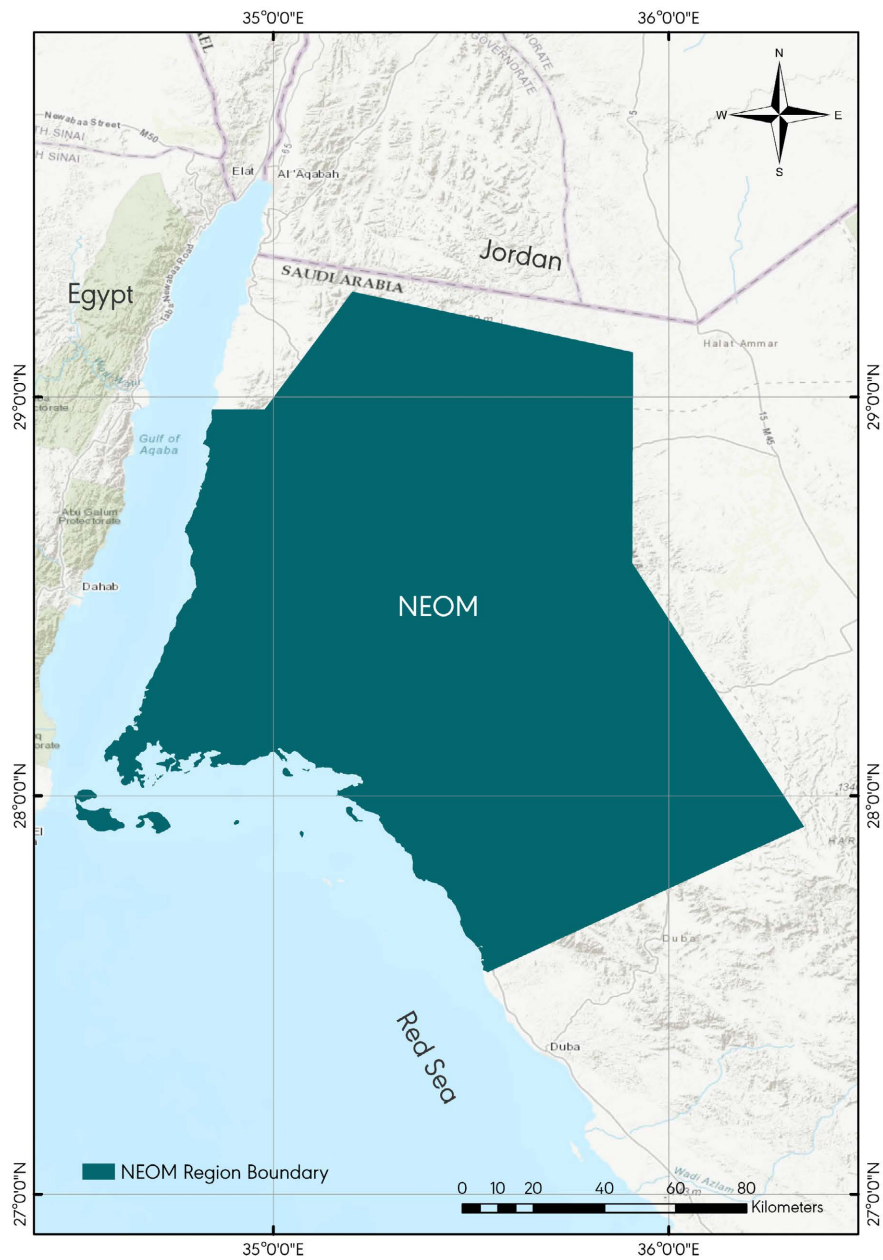


**Figure 1.** The study area of the NEOM region.

Several studies have used bivariate and multivariate statistical models to assess different aspects, such as [2] for Flash flood susceptibility assessment in Jeddah city, Kingdom of Saudi Arabia, [3] for a wind energy assessment for NEOM city, They also published an article titled “Landslide hazard assessment of the NEOM promising city, northwest Saudi Arabia: An integrated approach” [4]. A hybrid renewable energy system’s performance analysis and optimization for a sustainable NEOM city in Saudi Arabia aim to design and assess the performance of a Hybrid Renewable Energy System (HRES) for Saudi Arabia’s newly proposed grand city, NEOM [5].

An article titled Atmospheric conditions and air quality assessment over NEOM, Saudi Arabia [6] looked at the conditions (Atmospheric conditions and air quality assessment over NEOM, Saudi Arabia). A paper [7] studied the environment in a stand-alone hybrid PV-fuel cell-battery to desalinate seawater at Saudi NEOM city. Hydro-morphometric analysis of watersheds combined with remote sensing and geographic information system (GIS) techniques provides an effective tool for mapping and determining the areas’ most vulnerable to flood hazards and the levels of risk. Based on publicly available geological maps, ASTER and SRTM void-filled DEMs, Landsat 8 satellite imageries of the study area allowed extraction and calculation of morphometric basic, linear, areal, shape, and relief parameters for NEOM region watersheds. Flash flood hazard mapping is vital for catchment management (*i.e.*, for sustainable development of the water resources and protection from flood hazards and drought).

### 3. Data and Methods

According to [8], SRTM (30 meters) is the best DEM for studying basin hydrology and water resources. The results are comparable to Google maps and 1:50 k topographic maps. ASTER (30 meters) and SRTM (30 meters) are very close to each other, as are Google maps and topographic maps of 1:50 k. This study used SRTM digital elevation models to analyze hydrology in the NEOM region. These models are usually created in a GIS. The National Aeronautics and Space Administration (NASA) extended SRTM satellite products in 2000. It was first used to generate SRTM DEM to extract slope for the NEOM study area. This tool (SRTM) uses radar interferometry, where two radar images from slightly different locations are combined to produce digital topographic data for about 80% of the Earth’s land surface (USGS). Because SRTM (1 Arc-Second Global) with a resolution of 1-ARC (30 meters) was too large for ArcGIS Toolbox, we used SRTM (Void filled) with a resolution of 3-ARC (90 meters).

From launch to April 10, 2013, the satellite collected nearly 10,000 scenes Level-1 data set for Landsat 8 OLI/TIRS C1 (EarthExplorer). While these data are of the same quality and precision as data acquired after operational orbit, the geographic extent of each scene will vary, and most scenes will have full terrain correction with a 30-meter pixel size. The spatial resolution of early TIRS images may vary due to changes in telescope temperature.

### 3.1. Hydrology Analysis

Modeling water flow across a NEOM surface is helpful in many fields, including regional planning, agriculture, and forestry. These fields require knowledge of how water flows and how changes affect that flow. The ArcGIS Spatial Analyst extension's hydrologic analysis modeling tools help describe the physical components. Delineating watersheds and creating stream networks are all possible with hydrologic tools in the NEOM region. **Figure 2** shows an automated flow-chart process for a stream network generated from a digital elevation model.

This study used the hydrology tool in ArcGIS 10.8.1 to extract stream networks and watershed maps, and topographic maps were used to label watersheds. The Aerial Survey Department of the Ministry of Petroleum and Mineral Resources has produced topographic maps for Saudi Arabia as separate map sheets (scanned) (1984). Three scanned maps were collected for the NEOM study area: Tabuk, Duba, and Haqel. The topographic map sheets used to cover the NEOM are NH37-SW Tabuk, NH36-SE Haqel, and NH37-SW Duba (sheet: NG36-NE). Watersheds can be defined from a DEM by computing flow direction and using the Watershed tool. First, create a Flow Direction raster to find the contributing area with the Flow Direction tool. It must provide the locations to determine the catchment area.

Sources can be dams or stream gauges to determine the contributing area's characteristics. It may also use a flow accumulation threshold. The pour points are the stream network junctions created by flow accumulation when the threshold is used to define a watershed. Thus, a flow accumulation raster and the minimum number of cells that constitute a stream must be specified (the threshold value). The output is a raster of watersheds. When converting a raster dataset with area features, each group of adjacent cells with the same value becomes a polygon. Raster cell borders create arcs. The input raster's NoData cells do not become polygons. The input raster must be an integer raster dataset with any cell size. A raster dataset's attribute field will be used in the output feature class. If no field is specified in the output feature class attribute table, the input raster cell values (VALUE field) become a column with the heading Grid code.

### 3.2. Drainage Watersheds Delineation

As illustrated in **Figure 3**, the extraction of drainage watersheds from the analyzed SRTM Void filled DEMs is critical for quantitative studies in geomorphology and hydrology. The primary and most fundamental problem in extracting drainage networks is determining the flow direction of each cell in the digital elevation model, which fills in the cell gaps. Then, using ArcMap Toolbox, the flow network and directions were developed. There are 14 basins identified (Wadi Efal, Wadi Al Batinah, Wadi Ghurr, Wadi Sadr, Wadi Ayounah, Wadi Surr, Wadi Mabrak, Wadi Al Nakhlah, Ad Dubaysa, Wadi Umm Jarfeer, Wadi Haqaf, Wadi Al Zainah, Wadi Zawhi, and Wadi kamrah), as in **Table 1**.

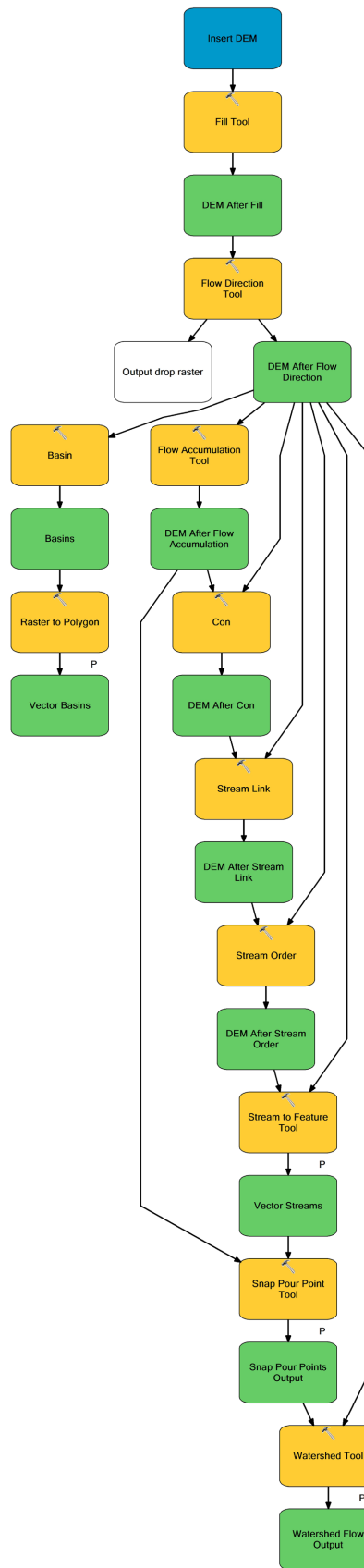


Figure 2. Hydrologic analysis model in ArcMap 10.8.1.



**Figure 3.** Watersheds delineation of the study area.

The length of the stream is greater in the first order, and it decreases as the stream order increases [9]. A long stream indicates a watershed with flatter gradients, while a short stream indicates a steep slope and delicate texture. The total length of the 14 watersheds' entire stream orders is 15038.65 kilometers (Figure 4). The first stream order contributes approximately 52.02% of the total stream length for the entire watershed, followed by the second stream order, which contributes 24.43 percent, the third stream order, which contributes 12.04 percent, the fourth stream order, which contributes 5.98 percent, the fourth stream order, which contributes 3.49 percent, the fifth stream order, which contributes 1.75 percent, and the seventh stream order, which contributes 0.28% (Table 2).

**Table 1.** Geometries of the delineated basins (for 5<sup>th</sup>. to 7<sup>th</sup>. Stream orders)

ID	Basins' Name	Area (km <sup>2</sup> )	Perimeter (km)	Hectares (ha)
0	Wadi Mabrak	369.18	106.63	36918.12
1	Wadi Umm Jarfeer	269.33	104.88	26933.27
2	Wadi Al Zainah	263.77	91.59	26377.28
3	Wadi Haqaf	265.85	93.99	26584.80
4	Wadi Efal	4992.17	477.21	499216.95
5	Wadi Al Nakhlah	276.75	103.16	27674.59
6	Wadi Al Batinah	2708.01	316.03	270800.83
7	Wadi Ayounah	824.78	182.61	82478.45
8	Ad Dubaysa	273.10	79.52	27309.80
9	Wadi Ghurr	1621.14	374.59	162113.53
10	Wadi Sadr	940.75	227.17	94074.95
11	Wadi Zawhi	223.10	94.43	22309.69
12	Wadi kamrah	104.93	66.25	10492.93
13	Wadi Surr	496.74	147.89	49673.82

**Table 2.** Stream order numbers and lengths of the watersheds.

ID	Basins' Name	1st. Stream Orders		2nd. Stream Orders		3rd. Stream Orders		4th. Stream Orders		5th. Stream Orders		6th. Stream Orders		7th. Stream Orders	
		Nu	Lu (km)												
0	Wadi Mabrak	188	210.53	76	74.60	34	31.59	66	57.06	7	4.78	-	-	-	-
1	Wadi Umm Jarfeer	136	164.07	72	81.43	20	27.18	31	22.56	9	5.27	-	-	-	-
2	Wadi Al Zainah	142	159.94	64	70.00	34	34.29	24	22.87	18	11.82	-	-	-	-
3	Wadi Haqaf	144	139.52	64	62.25	37	32.90	23	17.55	17	16.59	-	-	-	-
4	Wadi Efal	2572	2801.12	1218	1345.60	662	665.82	330	308.25	117	112.26	195	160.00	11	12.65
5	Wadi Al Nakhlah	148	183.46	76	77.84	26	35.83	15	10.17	25	21.19	-	-	-	-
6	Wadi Al Batinah	1398	1548.21	660	786.31	385	388.47	167	176.95	89	89.16	43	44.87	29	29.77
7	Wadi Ayounah	432	472.59	203	217.67	91	94.73	71	80.41	11	10.89	44	41.32	-	-
8	Ad Dubaysa	157	158.08	78	78.71	47	41.71	8	8.91	22	15.62	-	-	-	-
9	Wadi Ghurr	825	970.37	366	414.50	217	248.23	85	83.84	147	118.79	-	-	-	-
10	Wadi Sadr	491	538.06	224	248.82	132	123.90	60	55.24	59	50.88	10	17.56	-	-
11	Wadi Zawhi	124	120.84	58	58.92	35	36.03	3	2.42	23	20.19	-	-	-	-
12	Wadi kamrah	52	60.95	20	28.15	6	8.08	17	13.37	7	11.58	-	-	-	-
13	Wadi Surr	260	295.64	120	128.91	55	42.58	37	39.96	42	35.47	-	-	-	-

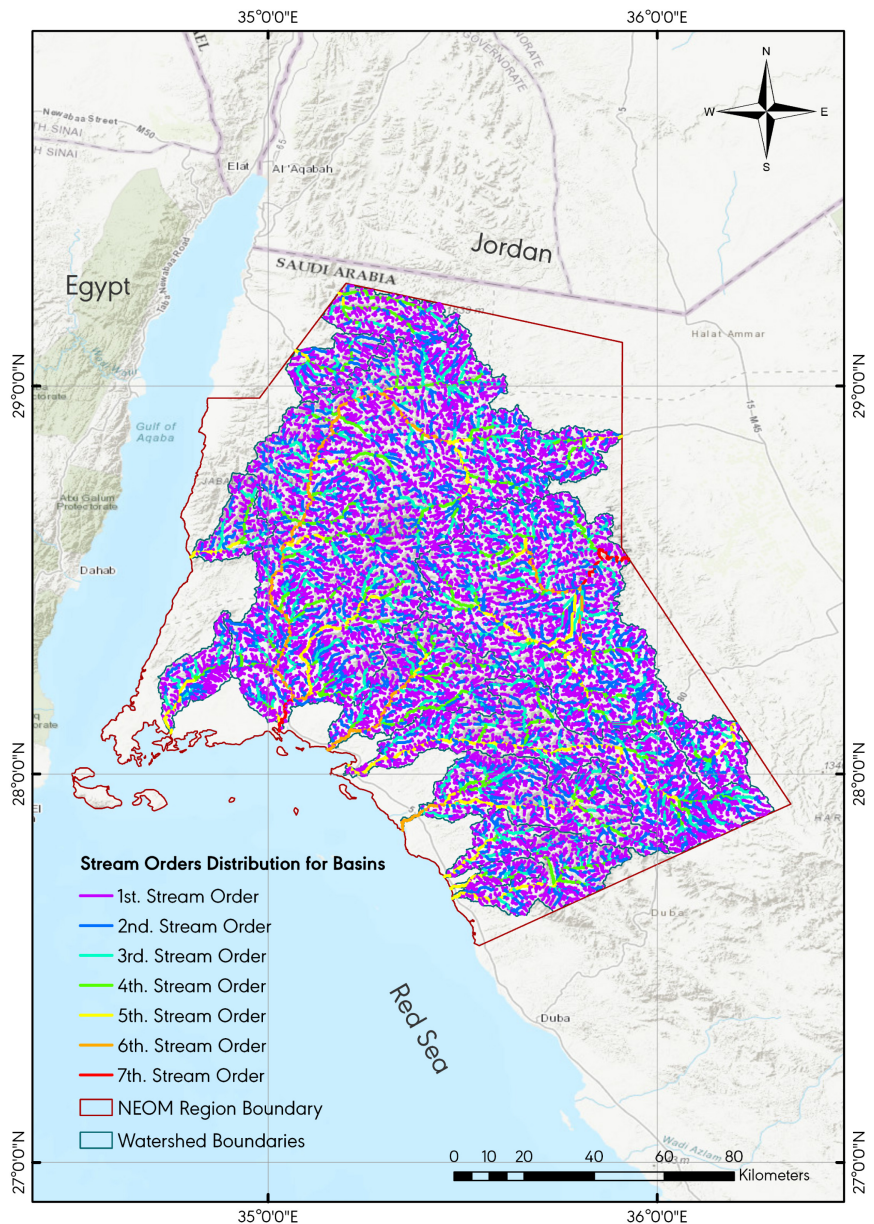


**Figure 4.** Stream orders distribution for basins map.

### 3.3. Morphometric Analysis

A quantitative morphometric analysis of the 14 watersheds in the NEOM region was carried out. For basin characterization, morphometric analyses were used in several articles. SRTM Void filled DEMs, ArcGIS 10.8.1 software, and the mathematical expressions shown in **Table 3** were used to extract and calculate 32 quantitative morphometric parameters. [10] [11] [12], and others. Different topographic features, such as aspects, slopes, and elevations, were generated using the Spatial Analyst tool. The following basic parameters are included: Perimeter (P), Basin Length (Lb), Stream order (Nu), Stream length (Lu), Mean Stream length (Rbm), Bifurcation ratio (Rb), Stream length ratio (Lurm), Rho Coefficient (R), Area (A), Drainage density (Dd), Stream Frequency (Fs), Drainage

**Table 3.** Computation of basic, derived, and shape morphometric parameters.

Aspects	Parameter	Formula	Unit	Reference
Linear	Perimeter ( $P$ )	GIS Software	km	Schumm (1956) [15]
	Basin Length ( $L_b$ )	GIS Software	km	Schumm (1956) [15]
	Stream order ( $N_u$ )	GIS Software	Dimensionless	Schumm (1956) [15]
	Stream length ( $L_u$ )	$N_u = N_1 + N_2 + N_3 + \dots + N_n$	km	Horton (1945) [16]
	Mean Stream length ( $Rbm$ )	$L_{sm} = \frac{L_u}{N_u}$	km	Horton (1945) [16]
	Bifurcation ratio ( $Rb$ )	$Rb = \frac{N_u}{N_{u+1}}$	Dimensionless	Horton (1945) [16]
	Stream length ratio ( $L_{urm}$ )	$L_{urm} = \frac{L_{ur}}{L_{u-1}}$	Dimensionless	Horton (1945) [16]
	Rho Coefficient ( $\rho$ )	$\rho = \frac{L_u}{R_b}$	Dimensionless	Horton (1945) [16]
Areal	Area ( $A$ )	GIS Software	km <sup>2</sup>	GIS Software
	Drainage density ( $Dd$ )	$Dd = \sum \frac{L_u}{A}$	km/km <sup>2</sup>	Horton (1945) [16]
	Stream Frequency ( $Fs$ )	$Fs = \frac{Nu}{A}$	Km <sup>-2</sup>	Horton (1945) [16]
	Drainage Texture ( $T$ )	$T = Dd \cdot Fs$	Km <sup>-1</sup>	Smith (1950) [17]
	Texture Ratio ( $Rt$ )	$Rt = \frac{N_u}{P}$	Km <sup>-1</sup>	Horton (1945) [16]
	Length of Overland Flow ( $Lg$ )	$Lg = \frac{1}{2} Dd$	km	Schumm (1956) [15]
	Constant of Channel Maintenance ( $CCM$ )	$C = \frac{1}{Dd}$	km	Schumm (1956) [15]
	Form factor ( $Ff$ )	$Rf = \frac{A}{(L_b)^2}$	Dimensionless	Horton (1932) [18]
	Circularity index ( $Rc$ )	$Rc = 4\pi \left( \frac{A}{P^2} \right)$	Dimensionless	Miller (1953) [10]
	Elongation ratio ( $Re$ )	$Re = \frac{\sqrt{A}}{L_b}$	Dimensionless	Schumm (1956) [15]
	Shape Index ( $Sw$ )	$Sw = \frac{1.27A}{(L_b)^2}$	Dimensionless	Haggett (1966) [19]
Compactness Coefficient ( $Cc$ )	$Cc = \frac{P}{2(\sqrt{\pi A})}$	Dimensionless	Horton (1945) [16]	
Infiltration Number ( $If$ )	$IF = Fs \cdot Dd$	Dimensionless	Faniran (1968) [20]	

Continued

Relief	Basin Relief ( $R$ )	$R = E - e$	m	Schumm (1956) [15]
	Relief Ratio ( $Rh$ )	$Rh = \frac{R}{L_b}$	Dimensionless	Schumm (1956) [15]
	Relative Relief ( $Rr$ )	$Rr = \frac{R}{P}$	Dimensionless	Melton (1957) [21]
	Ruggedness number ( $Rn$ )	$Rn = R \cdot Dd$	Dimensionless	Schumm (1956) [15]
	Gradient Ratio ( $G_r$ )	$Rg = \frac{Es - Em}{Lb}$	Dimensionless	Sreedevi <i>et al.</i> (2004) [22]
	Melton Ruggedness Ratio ( $MRn$ )	$MRn = \frac{H - h}{\sqrt{A}}$	Dimensionless	Melton (1965) [23]
	Lemniscate Shape ( $K$ )	$K = \frac{\pi(Lb)^2}{4A}$	Dimensionless	Chorley and Morley (1959) [24]
	Basin Slope ( $Sb$ )	$Sb = \frac{H - h}{Lb}$	Dimensionless	Miller (1953) [10]
	Channel Gradient ( $Cg$ )	$Cg = \frac{R}{\frac{\pi}{2 \cdot Lb}}$	m/km	Singh <i>et al.</i> (2014) [25]
	Hypsometric Integral ( $HI$ )	$HI = \frac{Elev - Elev_{min.}}{Elev_{max.} - Elev_{min.}}$	Dimensionless	Strahler (1957) [12]
Dissection Index ( $Di$ )	$Di = \frac{Rr}{Elev_{max.}}$	Dimensionless	Schumm (1956) [15]	

Texture (T), Texture Ratio (Rt), Length of Overland (Di). The morphometric hazard degree assessment method was used for eleven morphometric parameters that directly affect flash floods. Eight parameters have a directly proportional relationship with risk, while three others have an inverse proportional relationship with risk (Table 4). The hazard degree distributions for the basins of the NEOM region were calculated in order to:

- 1) The minimum and maximum values for the morphometric parameter for all basins in the NEOM region are determined.
- 2) A test to extract the empirical relationship between a basin's relative hazard degree in terms of flash floods and the morphometric parameters is used to assess the actual risk degree for all of the parameters that fall between their minimum and maximum values are used to assess the actual risk degree for all of the parameters that fall between their minimum and maximum values.
- 3) For parameters that have a directly proportional relationship to the degree of risk [13], the degree of hazard was calculated using the equations below:

$$\text{Hazard degree} = \frac{4(X - X_{min})}{X_{max} - X_{min}} + 1 \quad (1)$$

Similarly, the hazard degree is calculated using the following equation for parameters that have an inverse proportional relationship to the degree of risk:

**Table 4.** Calculation of ranks for morphometric parameters and the total rank value for the basins hazard assessment.

A	Direct Proportional Relationship						Inverse Proportional Relationship				Summation
	Dd	Fs	Rt	Rc	Rh	Rr	Rn	Lg	Re	Rb	
1.216	3.940	4.485	2.353	3.645	2.625	2.519	2.794	4.922	2.370	2.204	33.072
1.135	4.219	4.448	1.890	2.635	2.659	2.259	2.685	4.947	2.417	3.992	33.285
1.130	4.274	4.725	2.152	3.516	1.818	1.678	1.945	4.951	1.859	4.952	33.000
1.132	3.896	4.736	2.129	3.344	1.734	1.641	1.808	4.917	2.178	4.921	32.435
5.000	1.000	1.000	1.000	2.311	1.422	1.300	1.000	1.000	2.736	1.000	18.769
1.141	5.000	4.646	2.018	2.828	1.315	1.610	2.322	5.000	4.162	4.828	34.870
3.131	4.268	4.554	5.000	2.968	1.000	1.000	3.004	4.951	2.217	4.649	36.741
1.589	4.209	4.590	2.946	2.667	2.826	2.567	4.697	4.946	2.910	3.887	37.834
1.138	4.200	5.000	2.575	5.000	1.130	1.168	1.373	4.945	1.000	3.874	31.403
2.241	4.271	4.510	2.802	1.000	1.360	1.371	4.775	4.951	5.000	4.875	37.157
1.684	4.169	4.607	2.762	1.844	2.338	2.274	5.000	4.943	4.101	3.700	37.422
1.097	4.073	4.801	1.899	2.703	5.000	5.000	4.754	4.934	3.701	1.873	39.835
1.000	4.369	4.362	1.382	2.562	3.222	3.702	2.942	4.959	4.454	4.296	37.249
1.321	4.147	4.597	2.351	2.411	3.422	3.383	4.992	4.941	3.786	5.000	40.350

A = Area of Basin, Dd = Drainage Density, Fs = Stream Frequency, Rt = Drainage Texture Ratio, Rc = Circularity Ratio, Rh = Relief Ratio, Rr = Relative Relief, Rn = Ruggedness Number, Lg = Length of Overland Flow, Re = Elongation Ratio and Rb = Mean Bifurcation Ratio.

$$\text{Hazard degree} = \frac{4(X - X_{max})}{X_{min} - X_{max}} + 1 \quad (2)$$

$X_{min}$  and  $X_{max}$  are the minimum and maximum values of the morphometric parameters of the two basins and all basins, respectively, and  $X$  is the value of the morphometric parameters to be assessed for the hazard degree for each sub-basin. These basins' final flood hazard degree is the sum of the hazard degrees obtained from Equations (1) and (2) for each basin. Flash floods are directly proportional to basin area (A), drainage density (Dd), stream frequency (Fs), circularity index (Rc), relief ratio (Rh), relative relief (Rr), and ruggedness number (Rn). The higher the value of these parameters, the greater the risk of flooding, and watersheds with the highest value were ranked first. Inverse proportional relationships exist between the length of overland flow (Lg), elongation ratio (Re), and Mean Bifurcation Ratio (Rb). Based on the computed morphometric parameters, each watershed's total rank was determined and classified into five categories of flash flood susceptibility (Table 3). Very low hazard degree (18.769), low hazard (18.769 - 33.285), moderate (33.285 - 34.870), high hazard (34.870 - 37.834), and very high hazard (34.870 - 37.834) are the categories (37.834 - 40.350). Figure 5 depicts the final classification of the flash flood hazard degree map. According to the morphometric analysis calculations, the

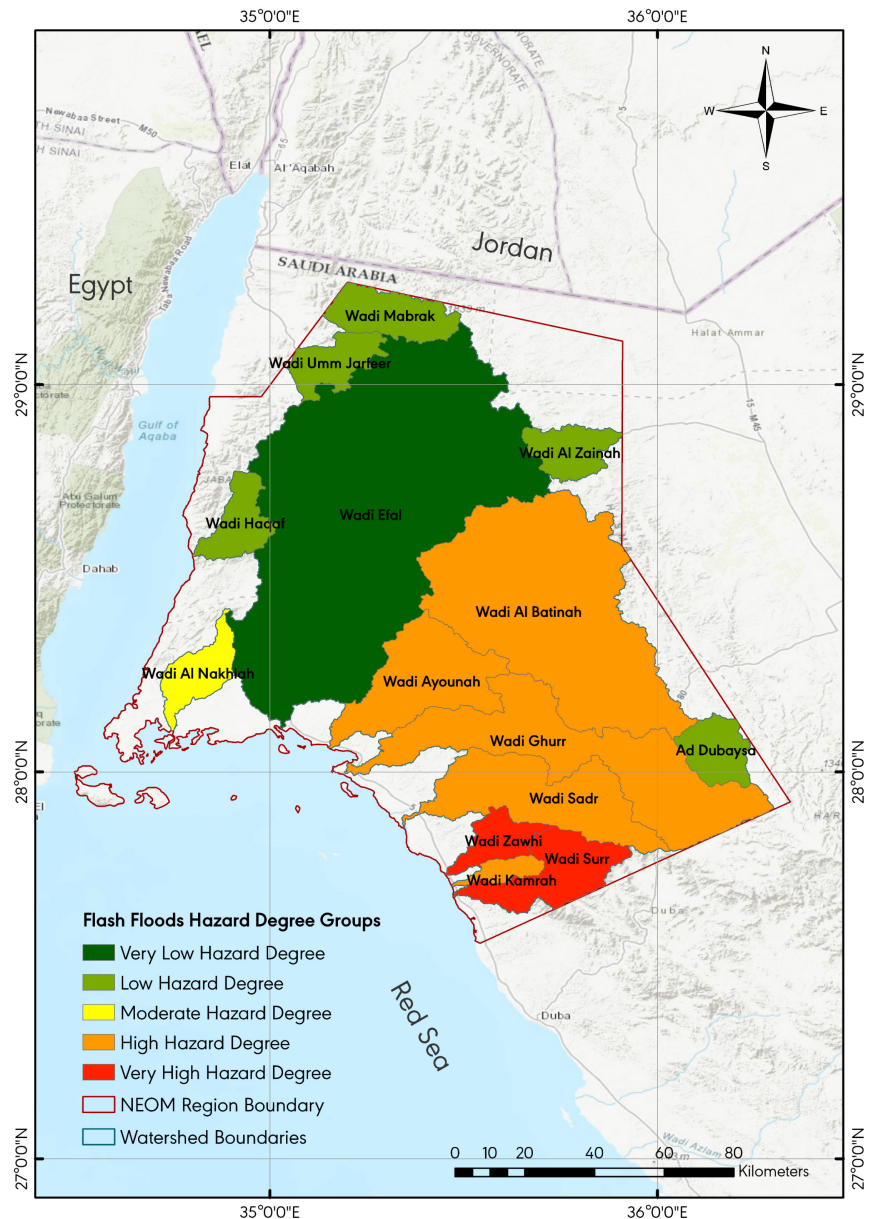


**Figure 5.** Classification of flash floods hazard degree map.

most dangerous degrees watersheds are (Wadi Zawhi) and (Wadi Zawhi) (Wadi Surr). The watersheds with the lowest hazardous degree have the largest catchment area (Wadi Efal). Finally, the flash flood hazard degree map was created by categorizing the results into five flooding susceptibility levels map: very low, low, moderate, high, and very high.

### 3.4. Remote Sensing (Digital Satellite Imagery Processing)

Landsat 8 Level 1 data products typically include both OLI and TIRS sensor data; however, the USGS archive may contain OLI- and/or TIRS-only scenes. All bands for the three satellite imageries were collected as close as possible to cover the entire study area of the NEOM region (2021-09-28 to 2021-11-08), and all

eleven bands can be used in conjunction with one another. Allowing for the display of artificial colors derived from different spectral bands aids in distinguishing between different surface features based on their reflection intensity. Some of the most frequently used band combinations on Landsat 8 are displayed in red, green, and blue (RGB) [14], as in **Figure 6**. MosaicPro is the mosaicking module for LPS, and ERDAS IMAGINE in the ERDAS IMAGINE software. It offers a robust solution for the entire mosaicking process, from seam generation and editing to radiometric adjustment and final product generation. (Release manual) ERDAS MosaicPro is beneficial for users of high-volume production who require an efficient method for editing seams on large projects involving large

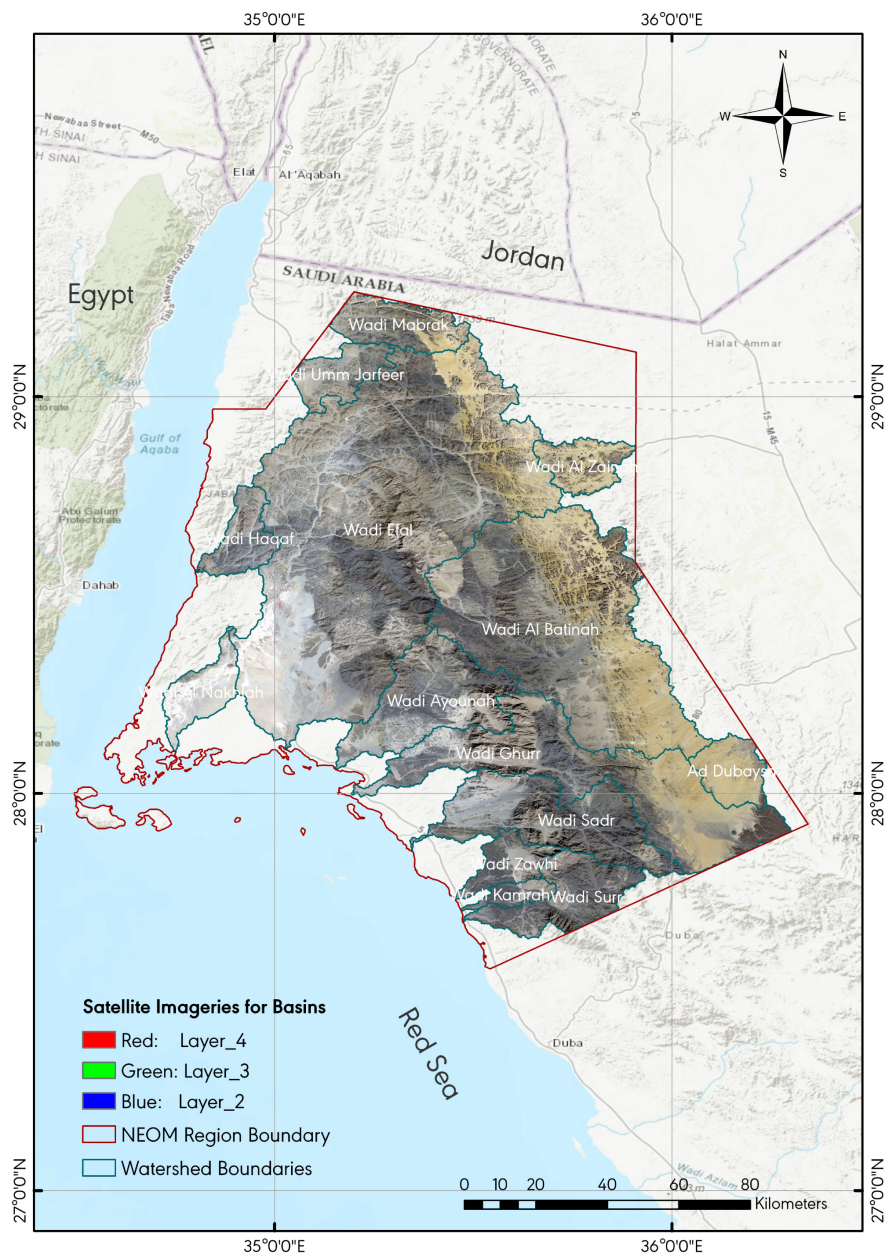


**Figure 6.** Satellite Imageries for NEOM basins map.

volumes of imagery. Seam editing can be carried out within the embedded ERDAS IMAGINE viewer, obviating the need to launch a separate viewer for cutline editing.

### 3.5. Flash Flooding Conditioning Factors

All input parameters were evenly scaled before the factors were integrated into weighted overlay analysis. Furthermore, all factors have been grouped according to their impact on flood susceptibility, and all parameters have been assigned a similar scale value. To ensure that the conclusions in this study were as accurate as possible, ten parameters that influence flash floods were included in the analysis. As a result, the following ten flash flood causal criteria were considered: Topographic wetness is determined by factors such as elevation (in meters), slope (in degrees), Stream Power Index (SPI), Topographic Roughness Index (TRI), Normalized Difference Vegetation Index (NDVI), Sediment Transport Index (STI), Stream Order, Flow Accumulation (Pixels), and Geological Formation. The SRTM 1 Void received Digital Elevation Models. Out of ten morphometric parameters, four were created with a 90-m spatial resolution. Thus, ArcGIS 10.8.1 software tools were used to calculate the values of the other five components (TWI, SPI, TRI, NDVI, and STI), while ArcGIS 10.8.1 software tools were used to collect the elevation, slope, stream order, and flow accumulation. Vector datasets extracted flash flood conditioning factors such as geological formation.

#### 3.5.1. Topographic Wetness Index (TWI)

TWI is a topo-hydrological factor that was first proposed by [26]. By controlling the spatial pattern of saturated areas, the TWI impacts hydrological processes at the watershed scale. The topographic wetness index [27] was developed as a critical component of the runoff model. The TWI is useful for determining the spatial distribution of wetness and contributing areas on upslope slopes. The formula is as follows:

$$TWI = \ln \left( \frac{\alpha}{\tan \beta} \right) \quad (3)$$

where  $\alpha$  represents the specific upslope area draining through a certain point per unit contour length ( $m^2 \cdot m^{-1}$ ), and  $\beta$  represents the slope grade (in degrees). In the research area, TWI values ranged from  $-7.49$  to  $18.84$  for Wadi Surr, and ranged from  $-7.37$  to  $11.08$  for Wadi Zawhi.

#### 3.5.2. Elevation

The most basic representation of a topological feature is elevation. Many previous flood risk assessment studies used the digital elevation model directly as an evaluation layer [28]. Low-lying areas are known to be more vulnerable to flooding than high-lying areas.

#### 3.5.3. Slope

Higher slopes result in faster flow rates and more water storage, putting the ter-

rain at risk of flooding and sediment transfer. When deciding where check dams should be built, consider the slope, as higher slopes are better for check dam construction [29]. The degree of elevation variation is reflected in the slope of adjacent grid cells, which were created in the shape of a grid using a computer model. The slope influences the flood. Because the water flows quickly in the steep slope area, the flood subsides quickly, reducing the risk of flooding. The steeper the terrain slope, the lower the area hazard [30]. Wadi Surr's slope ranged from 0 to 56.96, while Wadi Zawhi's slope ranged from 0 to 56.78.

#### 3.5.4. Stream Power Index (SPI)

Flood damage and river channel erosion have a significant impact on flow variables like stream power, shear stress, and velocity [31]. The SPI that represents stream power was chosen for the analysis. It is calculated as the product of catchment area and slope [32]:

$$SPI = A_s \tan \beta \quad (4)$$

The upstream area is denoted by  $A_s$ , and the cell slope is denoted by  $\beta$ . The SPI can locate suitable areas for soil conservation, reducing the impact of concentrated surface runoff [33]. SPI values in the research area ranged from 0 to 14.17 for Wadi Surr and 0 to 2.47 for Wadi Zawhi.

#### 3.5.5. Terrain Roughness Index (TRI)

The TRI is a critical factor affecting stream energy, surface storage capacity, runoff velocity, and routing (Rodríguez-Caballero, E., Cantón, Y., Chamizo, S., Afana, A., and Solé-Benet, A., 2012). The TRI is used to denote the elevation difference between adjacent cells [34], where the discrepancies between the focal cell and eight neighboring cells are determined as follows:

$$TRI = \gamma \sqrt{\sum (x_{ij} - x_{00})^2} \quad (5)$$

where  $x_{ij}$  is the height of each neighboring cell from cell to cell (0, 0), a flat terrain has no value, whereas a mountainous area with steep ridges has a positive value. The TRI values in the study area ranged from 0.11 to 0.83 in Wadi Surr and from 0.11 to 0.56 in Wadi Zawhi.

#### 3.5.6. Normalized Difference Vegetation Index (NDVI)

Another significant factor influencing flash flooding is the Normalized Difference Vegetation Index (NDVI). Indexes have values ranging from (negative 1) to (positive 1) [35]. According to [36], negative values represent water, and positive values represent vegetation; thus, NDVI has a negative correlation with flooding: higher NDVI values indicate a lower risk of flooding, while lower NDVI values indicate a higher risk of flooding. They were determined using the following equation:

$$NDVI = \frac{NIR - RED}{NIR + RED} \quad (6)$$

where *NIR* stands for near-infrared reflection and *RED* stands for red reflection.

The NDVI values for Wadi Surr range between  $-0.06$  and  $0.31$  in this study, while those for Wadi Zawhi range between  $-0.07$  and  $0.14$ .

### 3.5.7. Sediment Transport Index (STI)

Check dams have a variety of functions, including reducing sediment output and transporting sediment-associated pollutants to receiving bodies of water [37]. The STI can provide critical information about the potential for sediment transport through the stream network. It incorporates the effect of topography on erosion [33] and is thus used to characterize erosion and deposition processes [38], acting as a flood conditioning factor to define the movements of water-borne sediments due to water movement:

$$STI = \left( \frac{A_s}{22.13} \right)^{0.6} \times \left( \frac{\sin \beta}{0.0896} \right)^{1.3} \quad (7)$$

where  $A_s$  denotes the upstream area (*i.e.*, the area contributing to the upslope per unit contour length), while  $\beta$  denotes the slope at a specific cell. STIs ranged from 0 to 2749 in Wadi Surr, whereas STIs ranged from 0 to 1683 in Wadi Zawhi.

### 3.5.8. Stream Order

The classification of streams is based on the number of segments in each stream (1st, 2nd, 3rd, 4th, and 5th.). This reflects the stream's position in the ordering system [12]. The size and discharge capacity of a drainage basin, which affect flash flood threats, are determined by the order in which the streams flow through it. Wadis Surr and Zawhi were located in the fifth position in the stream sequence. Large streams are likely to emerge in these catchments, fed by a multitude of minor streams, resulting in significant water discharge and significant flow velocity depending on the relief conditions.

### 3.5.9. Flow Accumulation

Flood hazard is primarily defined by flow accumulation. The total volume of water flowing downslope into the output raster cells is called the accumulated flow. Accumulated flow values greater than a predefined threshold indicate areas of concentrated flow and thus a higher risk of flooding. The flow accumulation values in Wadi Surr range between 0 and 64,356, while those in Wadi Zawhi range between 0 and 29,103. Additionally, the outflow has the highest value. In lower-order streams, this component has lower values. The accumulation of flows was determined using the flow direction raster. Each cell in the flow accumulation raster contains information about the cells that flow into it, effectively acting as a discharge profile. An increase in flood susceptibility should accompany increased flow accumulation. The flow accumulation raster classes were designed to be as close to a river network's vector layer as possible.

### 3.5.10. Geological Formation

The French Geological Survey (BRGM), the United States Geological Survey (USGS), the Saudi Geological Survey (SGS), and the Deputy Ministry for Miner-

al Resources conducted geologic mapping at a scale of 1:250,000 between 1974 and 2011 (DMMR). The dataset includes data on the Arabian Shield's lithologic units. Between 1977 and 2019, each map sheet was published. In 2008, the data were digitized and combined into a single geological dataset, as illustrated in **Figure 7**. Geologic mapping observations were made in the field and located and positioned using KSA's 1:500,000 map, 1:250,000 base or topographic maps, aerial photographs at various scales, or 1:60,000 aerial maps. Between 1977 and 2019, observation points were also located using a GPS instrument with a precision of greater than 10 meters. The SGS Geological Survey's map observation and borehole databases recorded observations. Along with the airborne magnetometer, the Landsat image provides a higher level of interpretability.

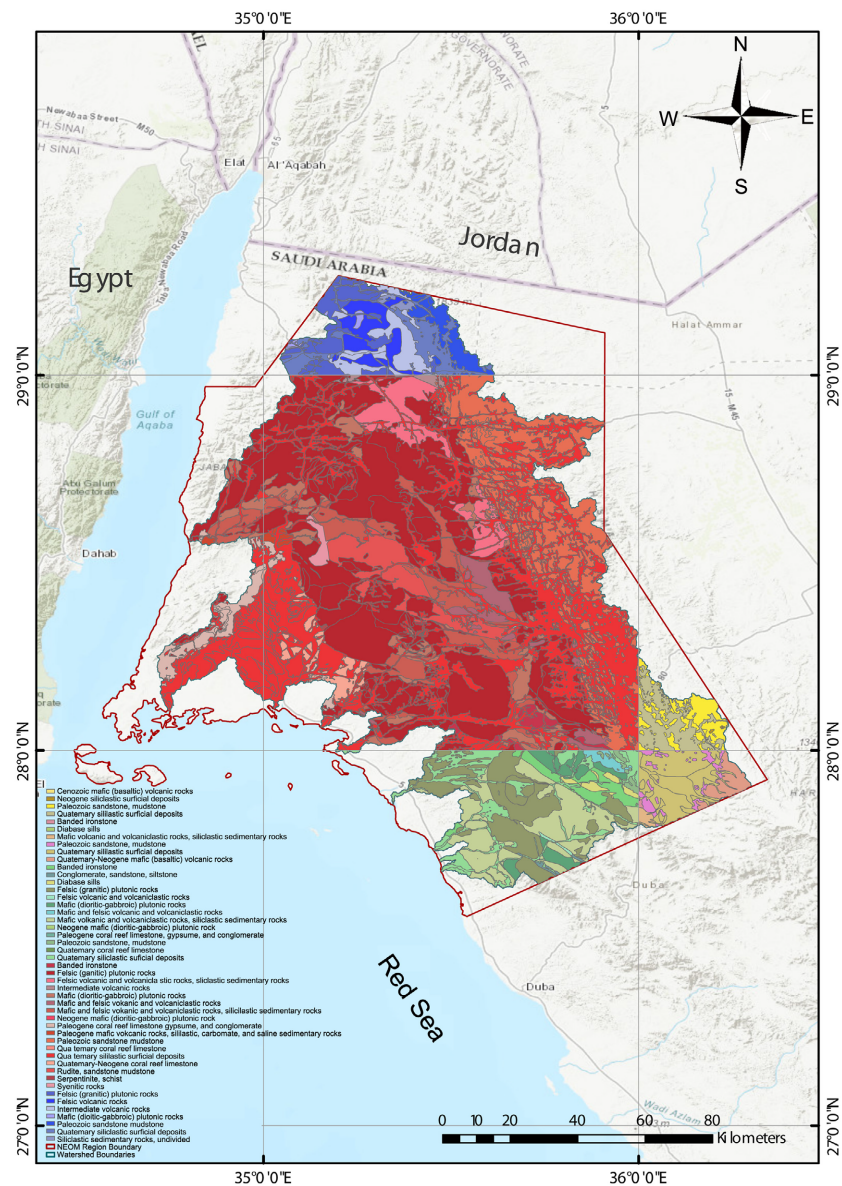


**Figure 7.** Geological formation of NEOM region watersheds. source: Saudi geological survey.

### 3.6. Analytical Hierarchy Process (AHP)

The AHP is a versatile tool that ranks both criteria and user options pairwise. The AHP is a tool that can translate qualitative and quantitative judgments into a multi-criteria ranking. The evaluation process may become arbitrary because the AHP only requires the decision-maker to compare two options or criteria. With more criteria and alternatives, the number of pairwise comparisons increases quadratically (Figure 8). To solve a complex decision problem, [39] invented AHP, which divides it into smaller units, resolves them, and then reassembles them. It is used to make decisions based on expert judgment. The dominant AHP establishes priority scales based on specialist judgment; it is used to make decisions based on expert judgment. According to [39], if the consistency ratio exceeds 0.1, the set of judgments is not reliable. This study evaluated the ten conditioning factors for flash flood susceptibility in Wadis Surr and Zawhi. So, a 10x10 matrix was made. Using this matrix, the normalized primary eigenvector was calculated in three steps. To create the relative weight matrix, the values of  $j$  (column) were added together, and then each element was divided by the sum. The normalized primary eigenvector was computed by averaging the rows. The resulting factor weights were normalized by multiplying 100 (Figure 9). When comparing two comparisons, the consistency ratio ( $CR$ ) must always be less than 0.1 [39]. If the ratio is greater than 0.10, the matrix should be re-evaluated. The following formula is used to determine the consistency ratio:

$$CR = \frac{CI}{RI} \tag{8}$$

where  $CI$  stands for consistency index and  $RI$  stands for random consistency index.

$$CI = \frac{\lambda_{max} - n}{n - 1} \tag{9}$$

where  $n$  is the number of comparisons and  $\lambda_{max}$  is the major eigenvalue, the random consistency indices used to determine the consistency ratio were chosen

Matrix											normalized principal Eigenvector
	TWI	Elevation	Slope	SPI	TRI	NDVI	STI	Stream Order	Flow Accum.	Geology	
TWI	1	1/3	1/3	1/3	1	1/2	2	1/4	1/5	1/3	3.78%
Elevation	3	1	1/3	1	3	2	5	1/3	1/2	1	9.48%
Slope	3	3	1	2	4	3	3	1/3	1	1	14.56%
SPI	4	3	1	1/2	1	4	1	3	1	2	13.08%
TRI	5	1	1/3	1/4	1/4	1	1/2	2	1/7	1/3	3.48%
NDVI	6	2	1/2	1/3	1	2	1	5	1/3	1/2	7.20%
STI	7	1/2	1/5	1/3	1/3	1/2	1/5	1	1/9	1/3	2.53%
Stream Order	4	3	3	1	7	3	9	1	2	3	23.40%
Flow Accum.	5	2	1	1/2	3	2	6	1/2	1	1	12.60%
Geology	3	1	1	1/2	3	2	3	1/3	1	1	9.90%

Figure 8. Matrix of pairwise comparisons for factor criteria.

0.04	0.03	0.04	0.04	0.04	0.03	0.05	0.06	0.02	0.03
0.12	0.08	0.04	0.13	0.11	0.13	0.13	0.08	0.06	0.10
0.12	0.24	0.12	0.25	0.14	0.20	0.08	0.08	0.11	0.10
0.12	0.08	0.06	0.13	0.14	0.07	0.08	0.23	0.23	0.19
0.04	0.03	0.03	0.03	0.04	0.03	0.05	0.03	0.04	0.03
0.08	0.04	0.04	0.13	0.07	0.07	0.13	0.08	0.06	0.05
0.02	0.02	0.04	0.04	0.02	0.01	0.03	0.03	0.02	0.03
0.16	0.24	0.37	0.13	0.25	0.20	0.23	0.23	0.23	0.29
0.20	0.16	0.12	0.06	0.11	0.13	0.15	0.12	0.11	0.10
0.12	0.08	0.12	0.06	0.11	0.13	0.08	0.08	0.11	0.10
1.00	1.00	1.00	1.00	1.00	1.00	1.00	1.00	1.00	1.00

Figure 9. Normalizing the columns of flash flood criteria.

at random. For the theme layers that were employed in the flash floods susceptibility site selection, the consistency check values are:  $\lambda_{max} = 10.571$ ,  $CI = 0.154959$ , number of factors = 10,  $CR = 0.042773$ , which is significantly less than the threshold level of 0.10.

### 3.7. Weighted Index Overlay

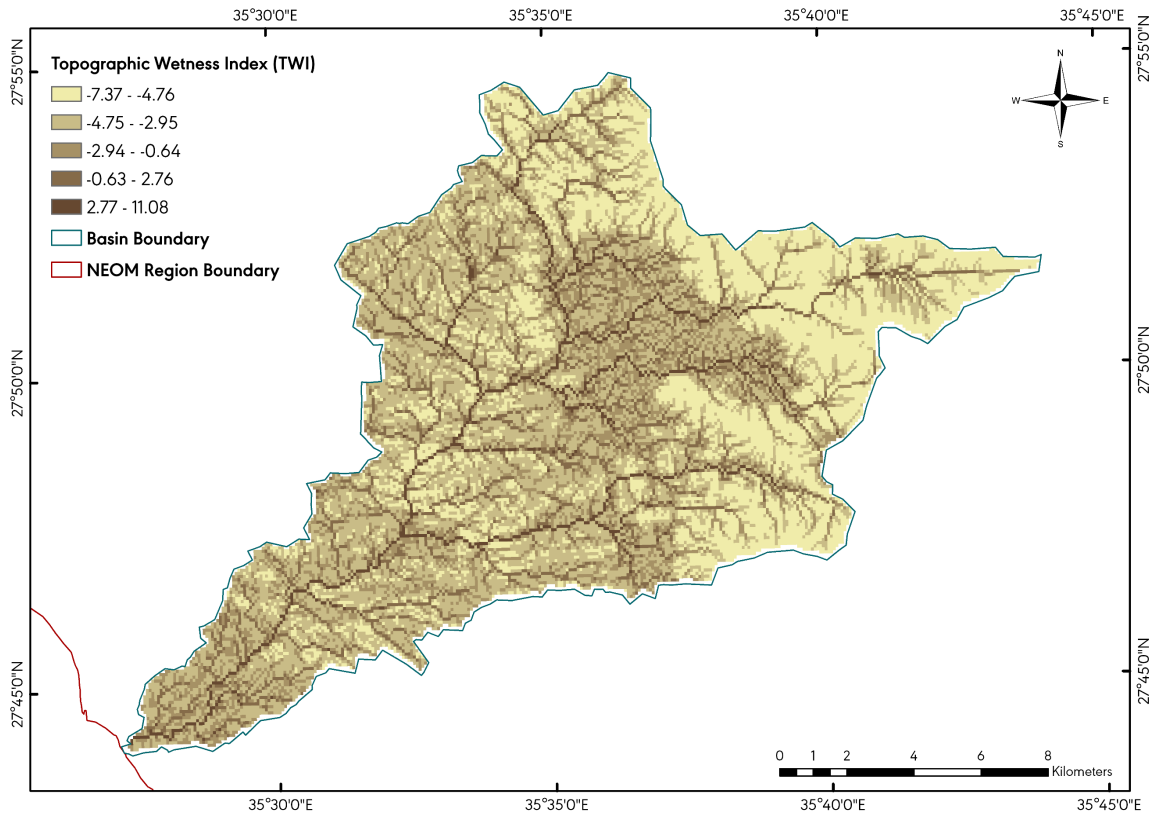
Weighted index overlay analysis is a straightforward technique for integrating multiple class maps in order to accomplish a specific goal. This technique enables the investigation to incorporate human judgment based on acquired knowledge and experience. The weights assigned in this table indicate the relative importance of each element to the overall objective. Most importantly, it takes into account the factors' relative importance as well as their unique characteristics. Because this technique lacks a defined scale, the study's weighting criteria were developed and implemented using the AHP analysis. The ten themed maps were layered using a weighted index overlay to identify the areas most prone to flash floods (Equation (10)).

$$S = \frac{\sum w_i s_{ij}}{\sum w_i} \tag{10}$$

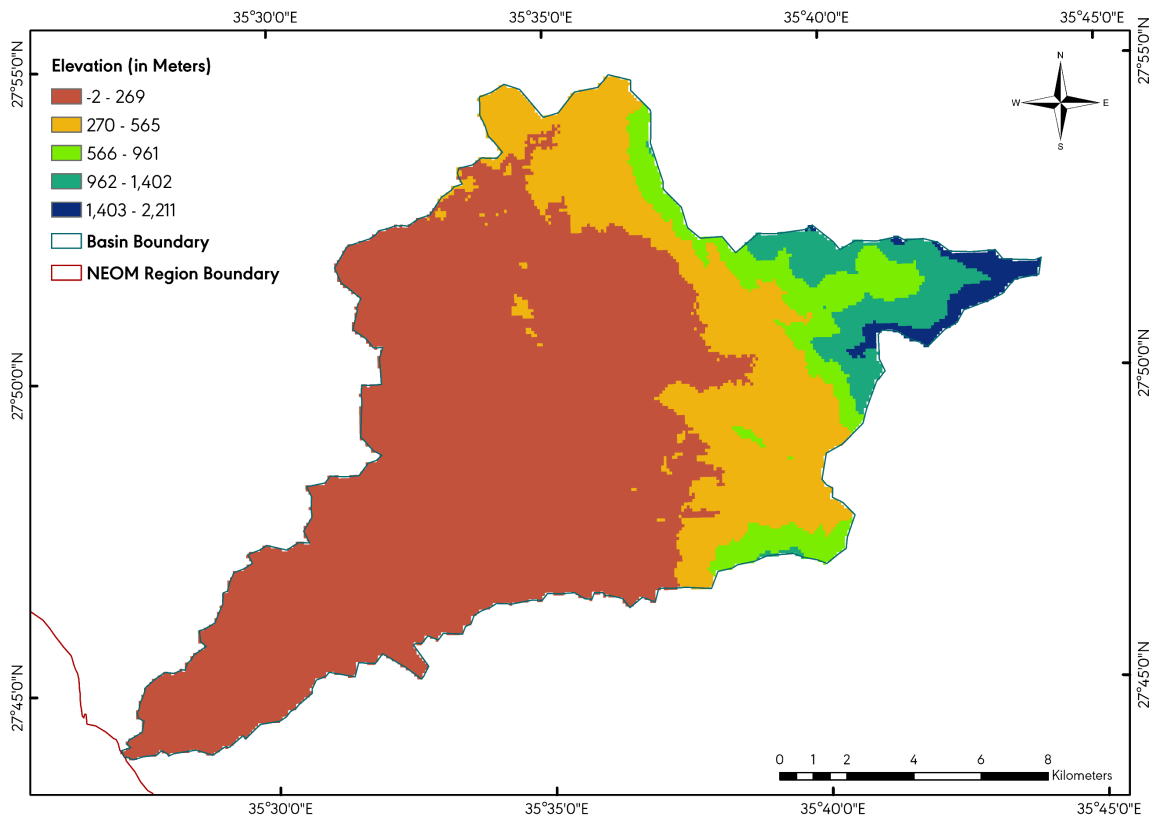
where  $w_i$  is the weight of the  $i$ th factor map,  $s_{ij}$  is the spatial class weight of the  $j$ th factor map, and  $s$  is the value of the spatial unit of the output map. Each criterion's relative importance (priority) concerning the others is established here. The importance values assigned in this study were determined by comparing each criterion to all others. Figure 8 and Figure 9 compare the weights assigned to the ten criteria.

## 4. Results and Discussion

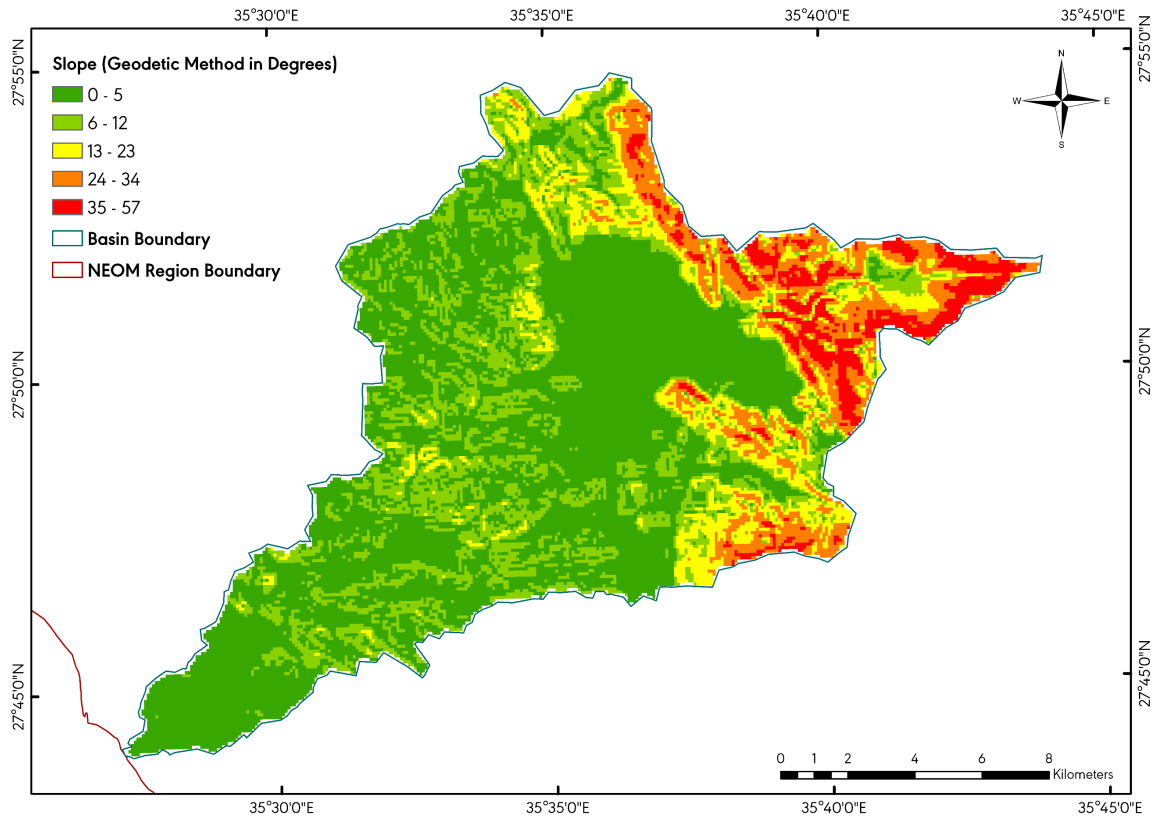
Topographic wetness index (TWI), elevation, slope, stream power index (SPI), topographic roughness index (TRI), normalized difference vegetation index (NDVI), sediment transport index (STI), stream order, flow accumulation, and geological formation are among the ten factors taken into account in the current study's assessment of flash flood hazards throughout the NEOM region. Using GIS techniques, the flash flood susceptibility danger map was constructed by transforming each factor into a raster grid cell. Table 5 sorted each factor layer by relevance. Figure 10 and Figure 11 demonstrate each significant factor's



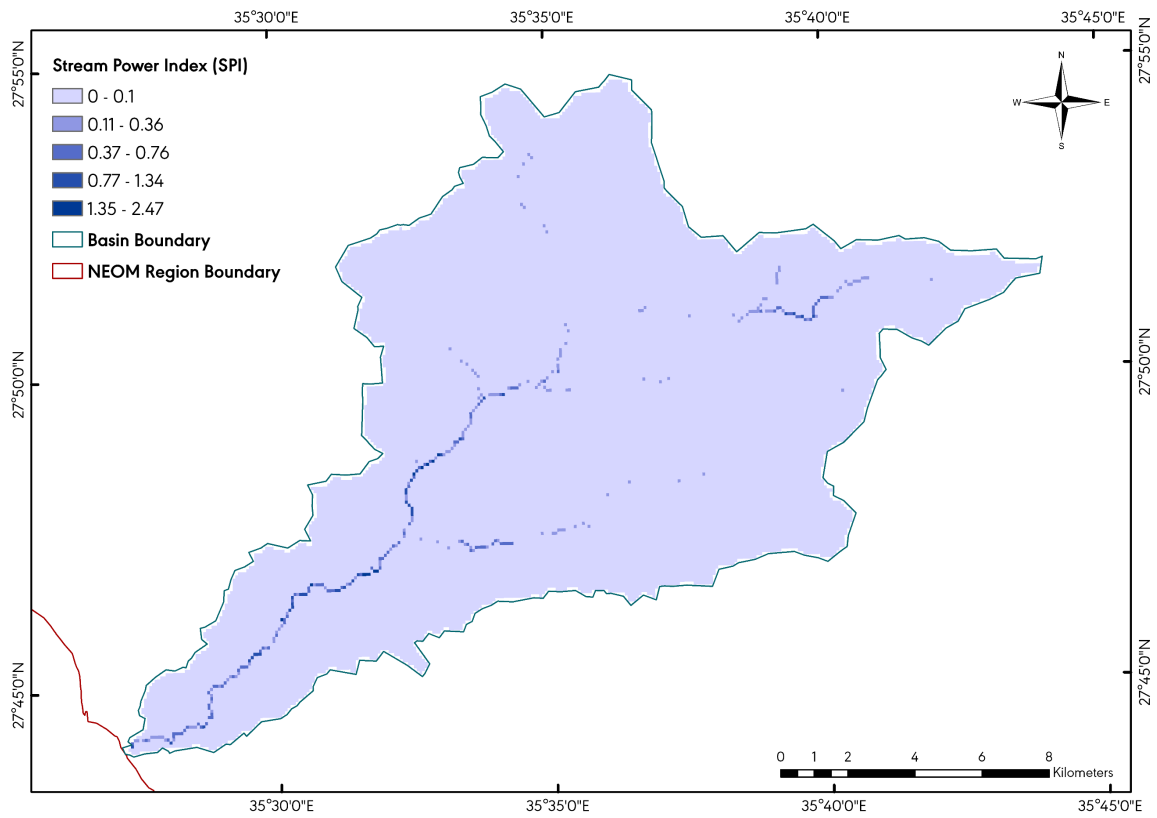
(a)



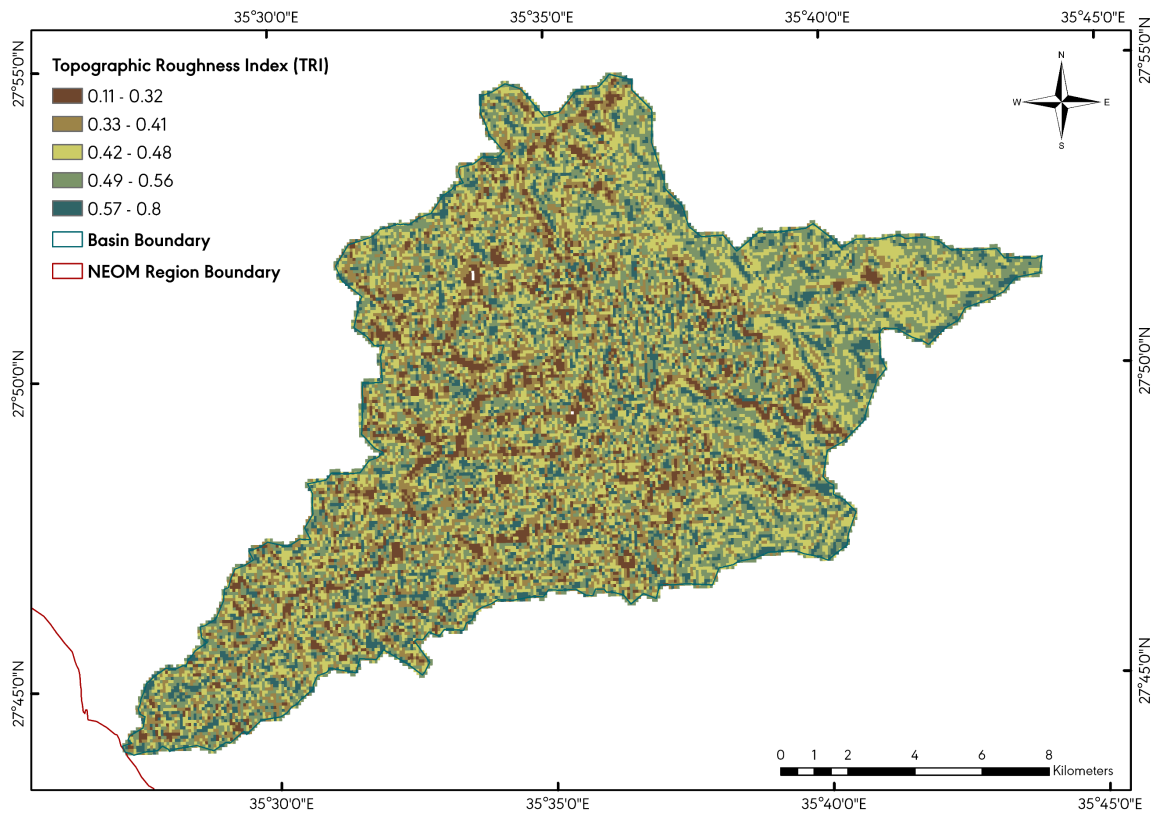
(b)



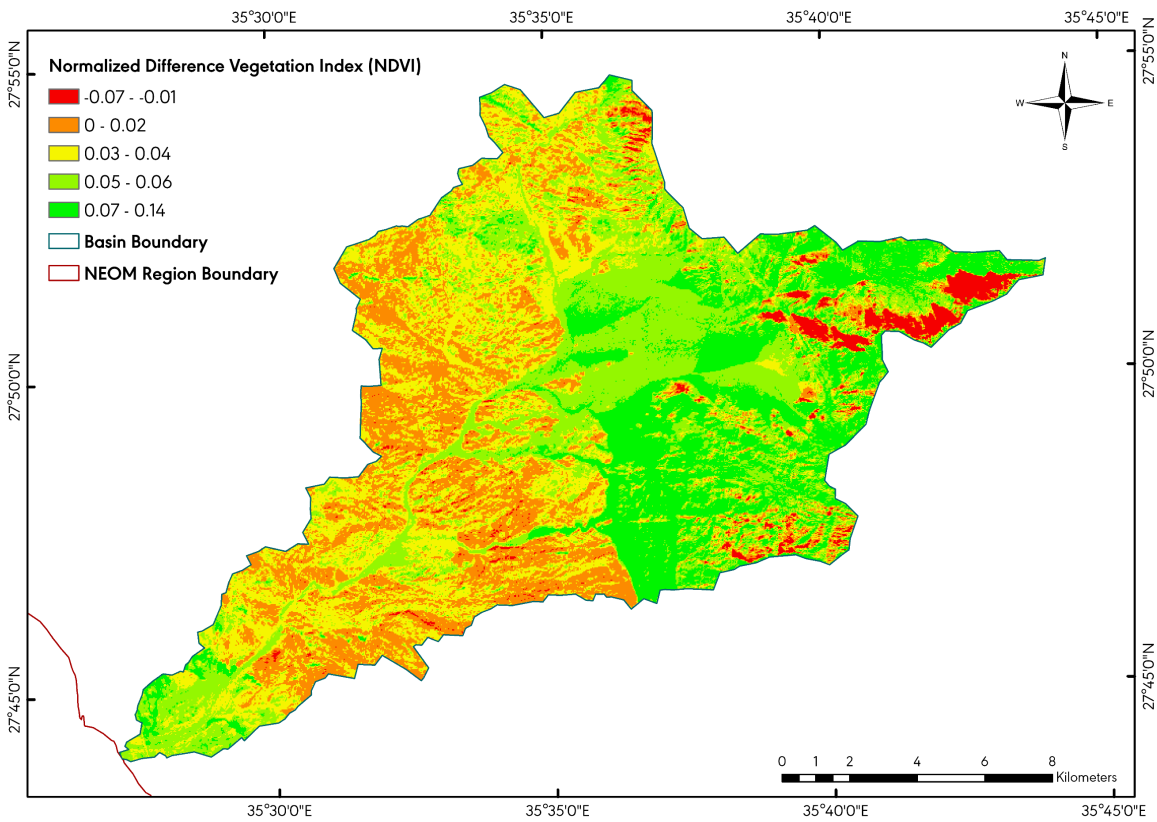
(c)



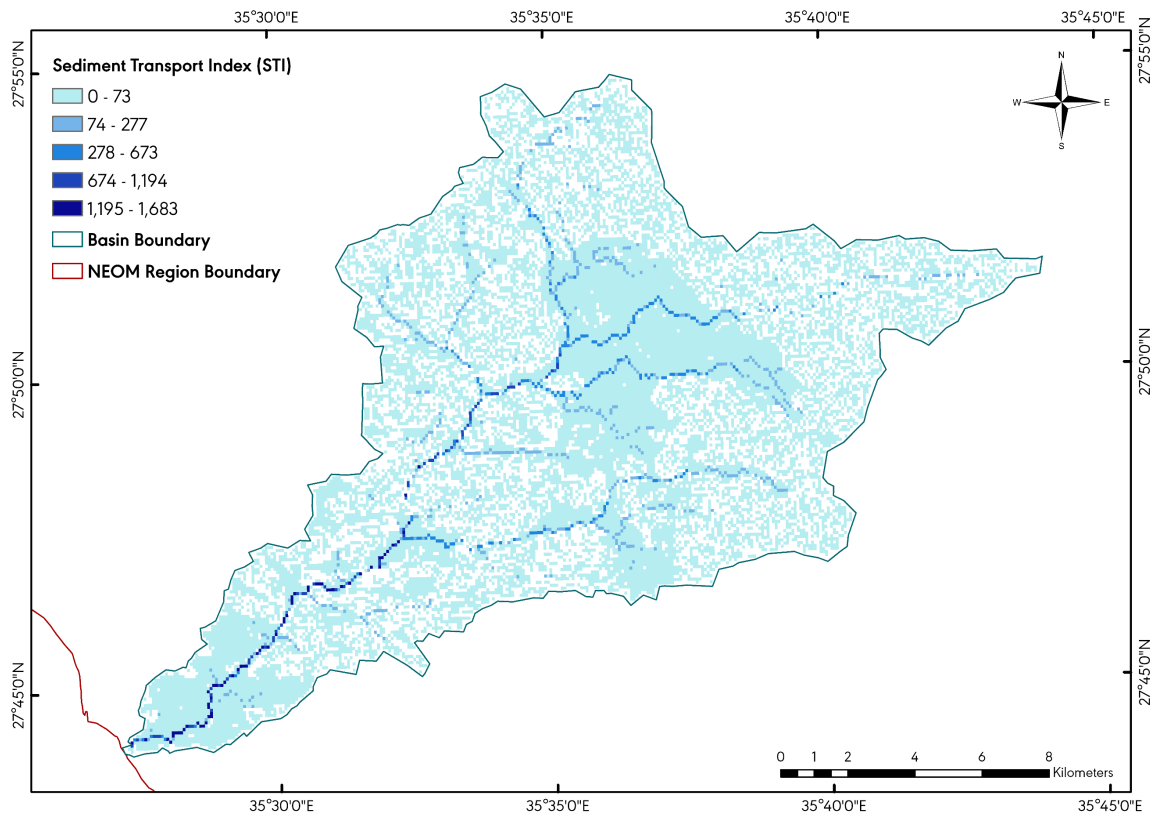
(d)



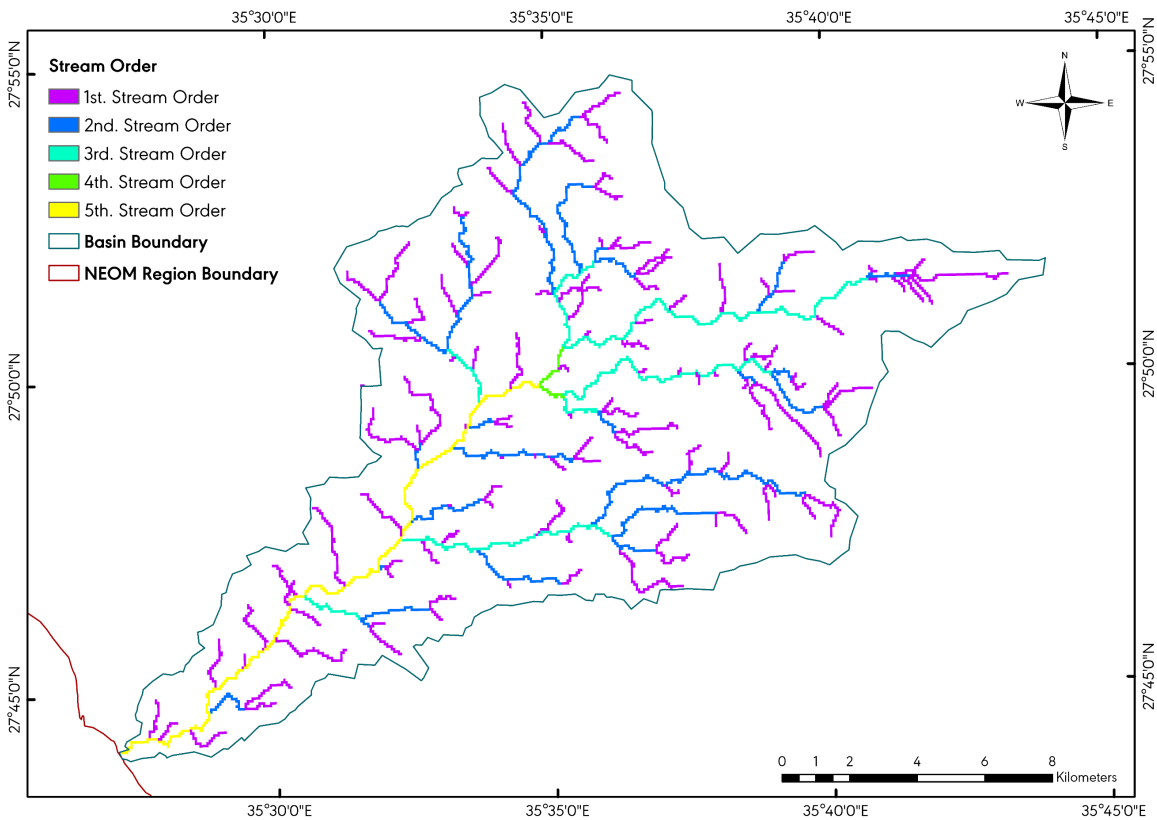
(e)



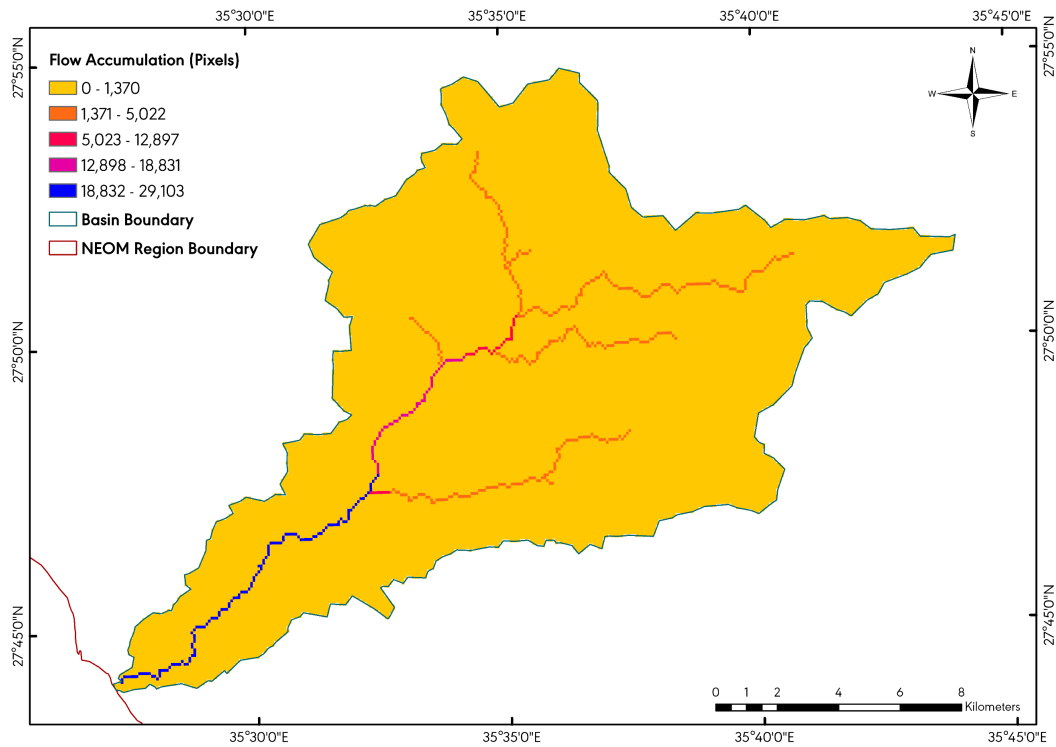
(f)



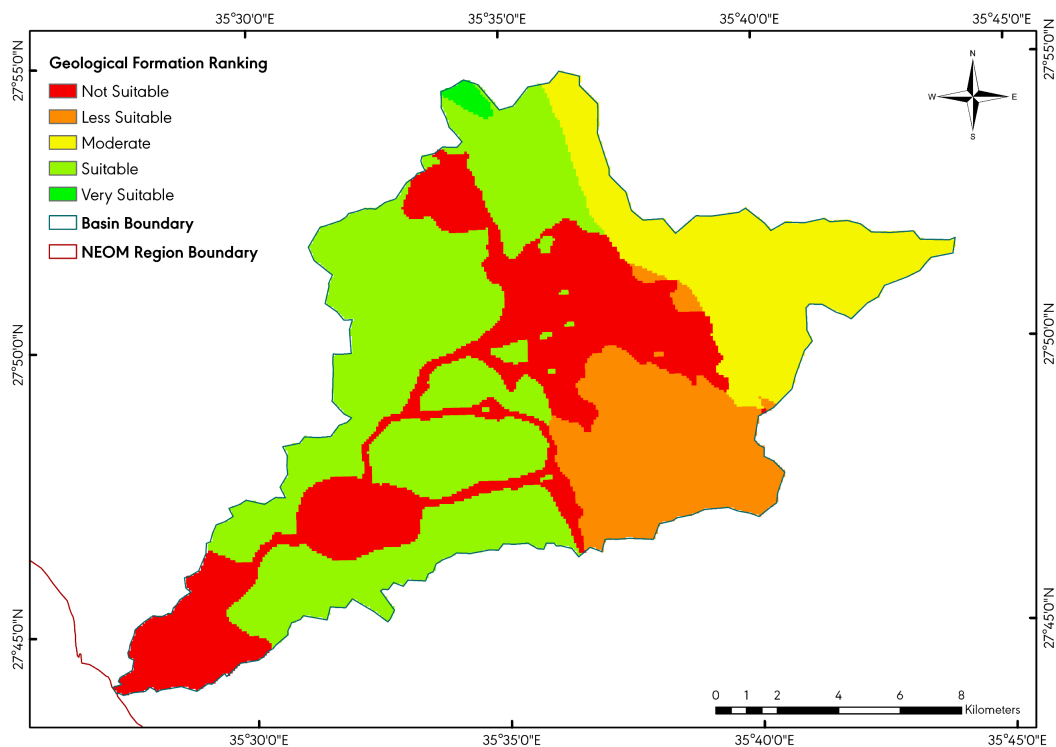
(g)



(h)

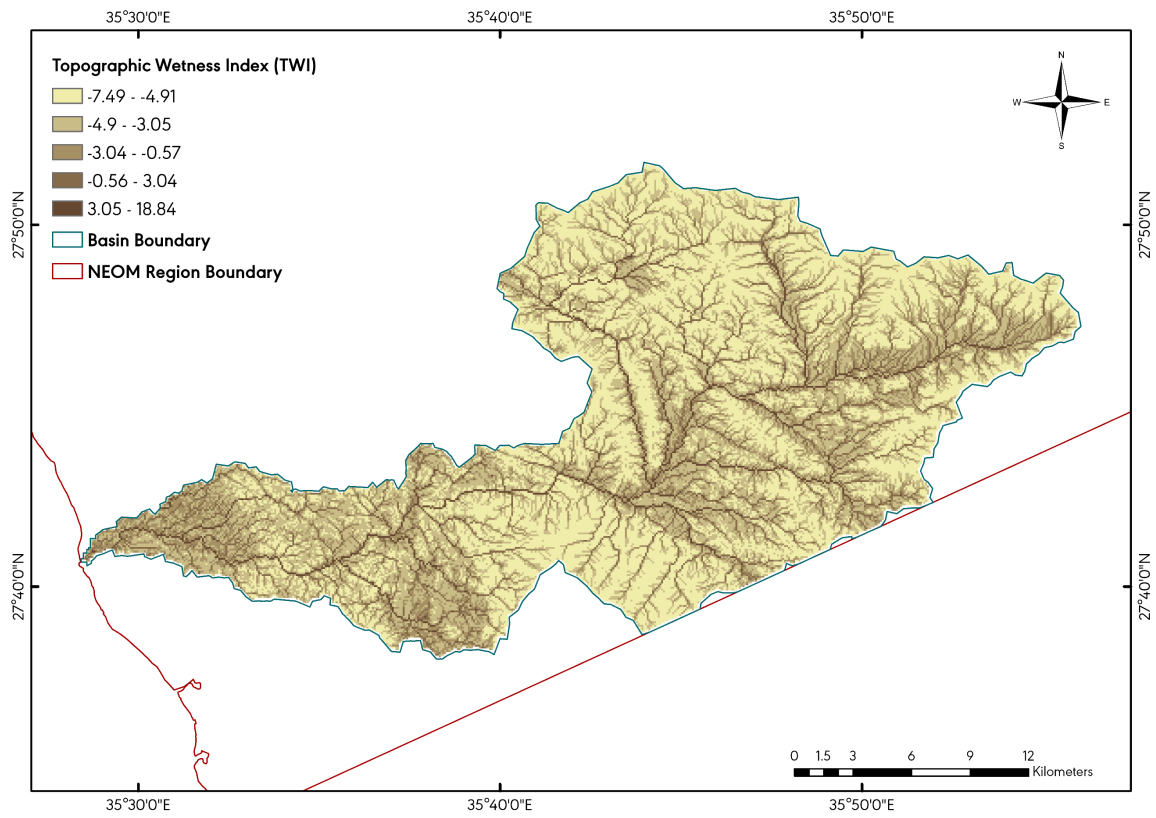


(i)

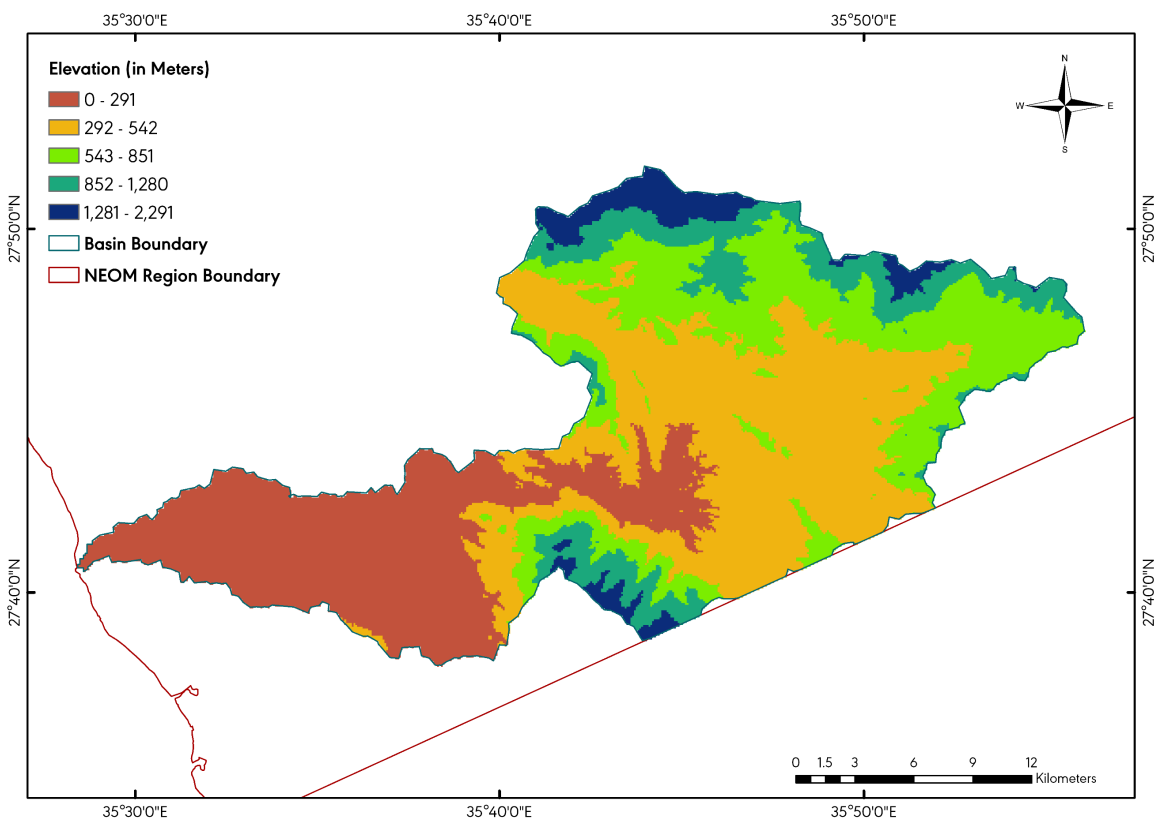


(j)

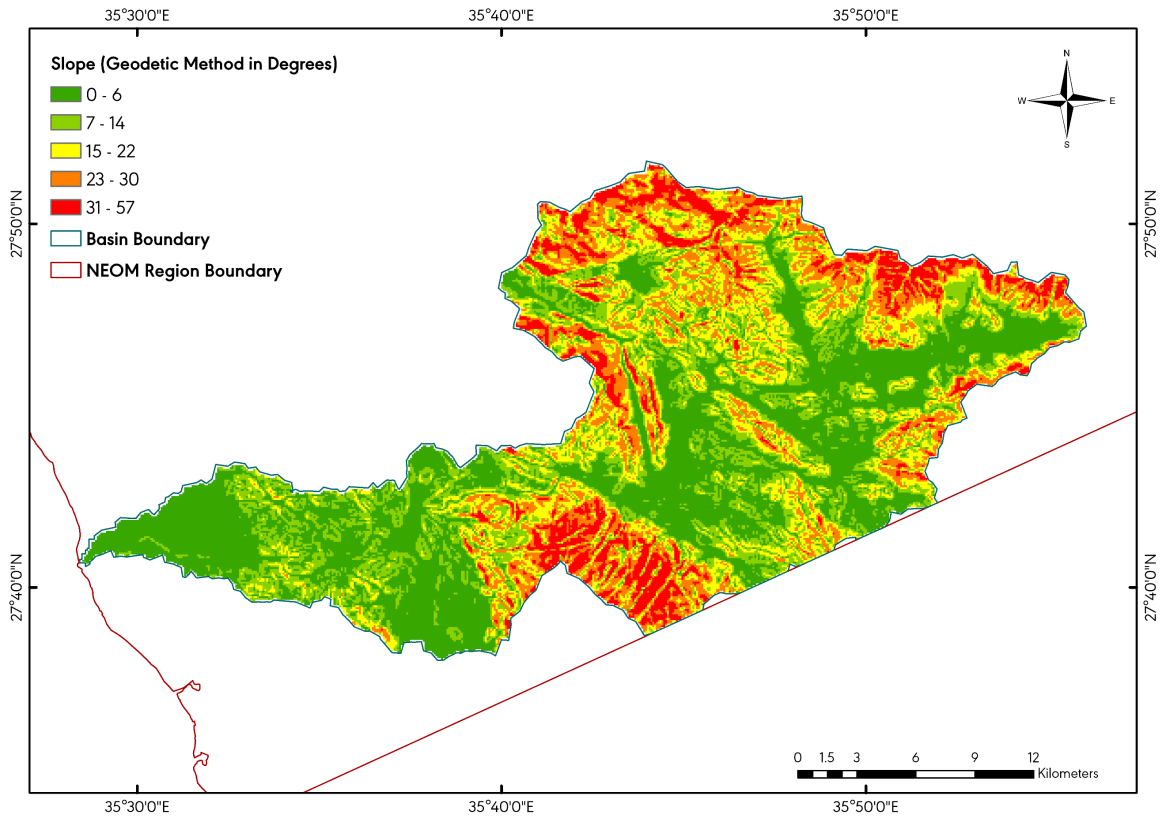
**Figure 10.** Influencing ten Wadi Zawhi flash flood causative criteria, including (a) Topographic Wetness Index (TWI), (b) Elevation, (c) Slope, (d) Stream Power Index (SPI), (e) Topographic Roughness Index (TRI), (f) Normalized Difference Vegetation Index (NDVI), (g) Sediment Transport Index (STI), (h) Stream Order, (i) Flow Accumulation, and (j) Geological Formation Ranking.



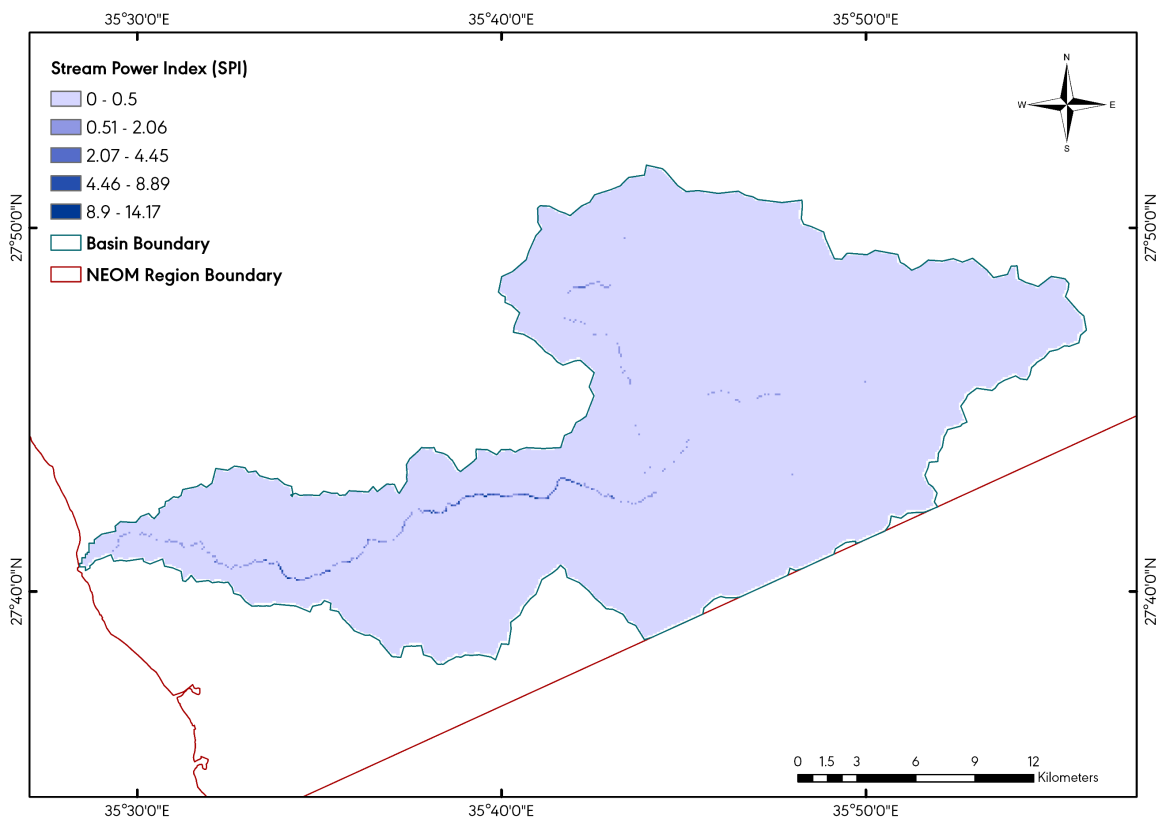
(a)



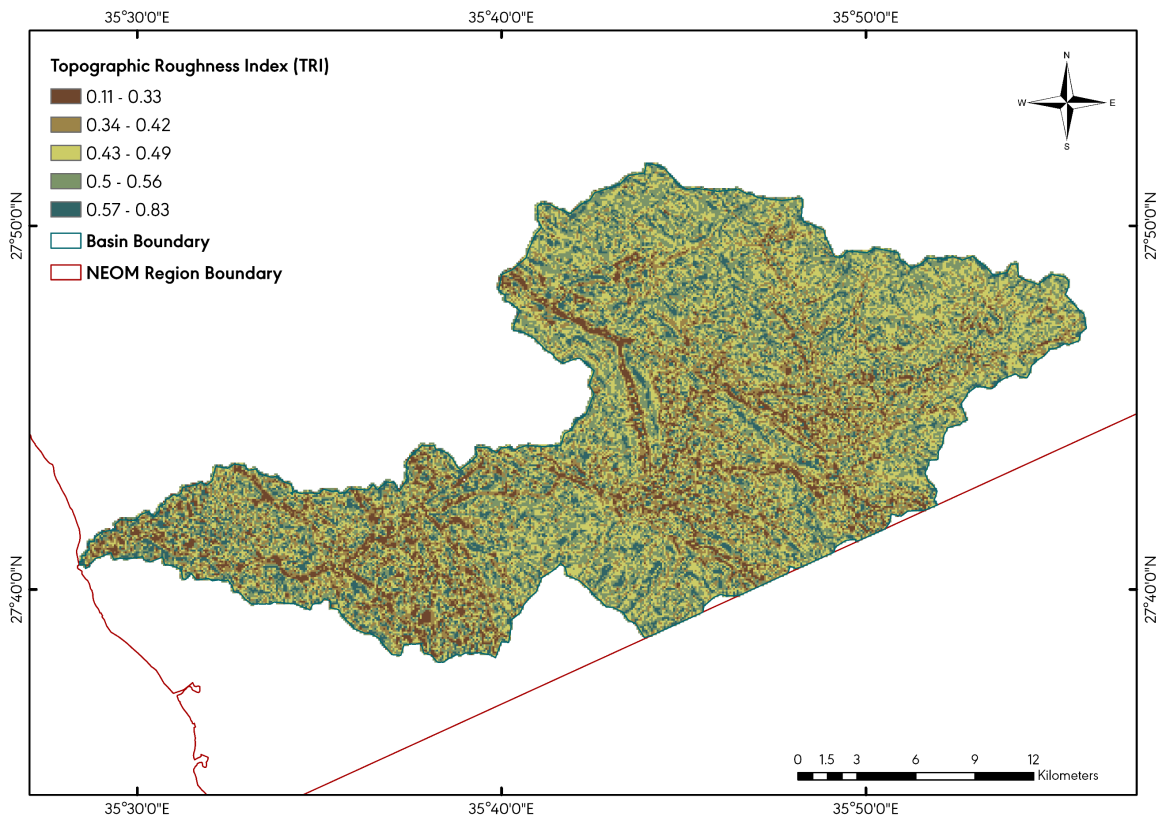
(b)



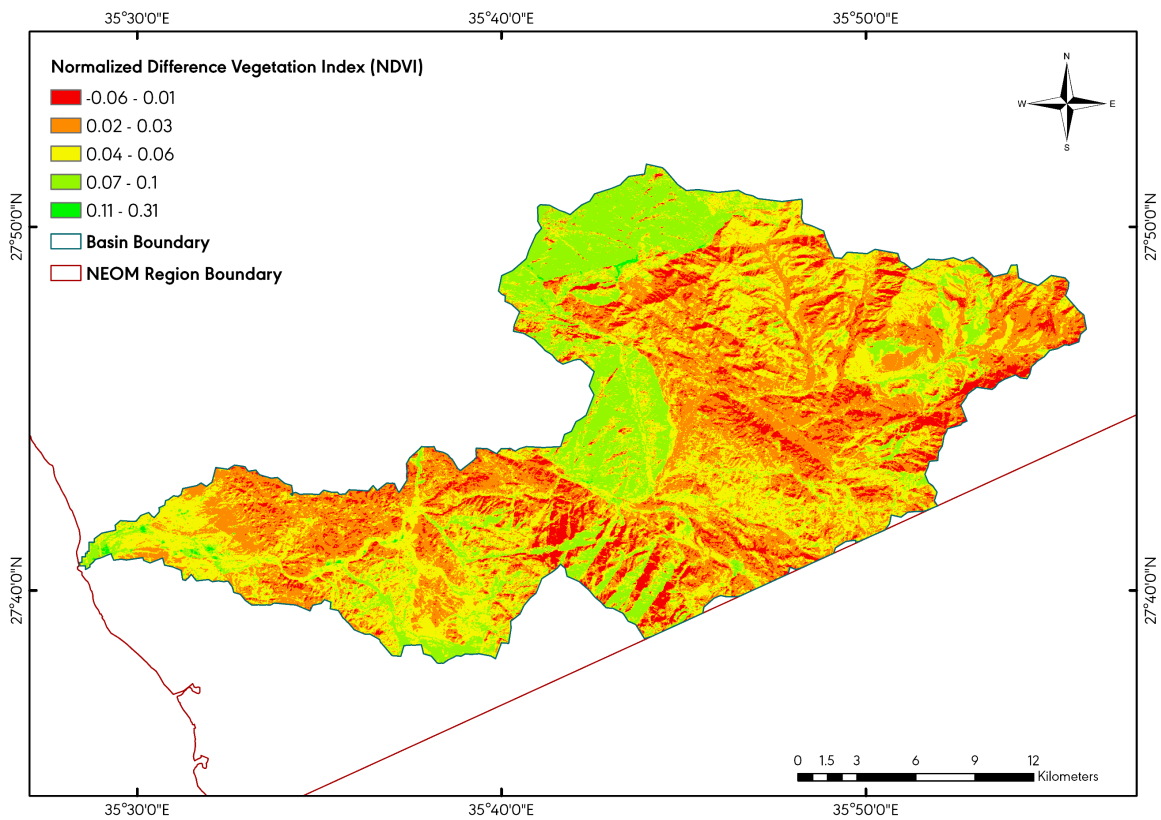
(c)



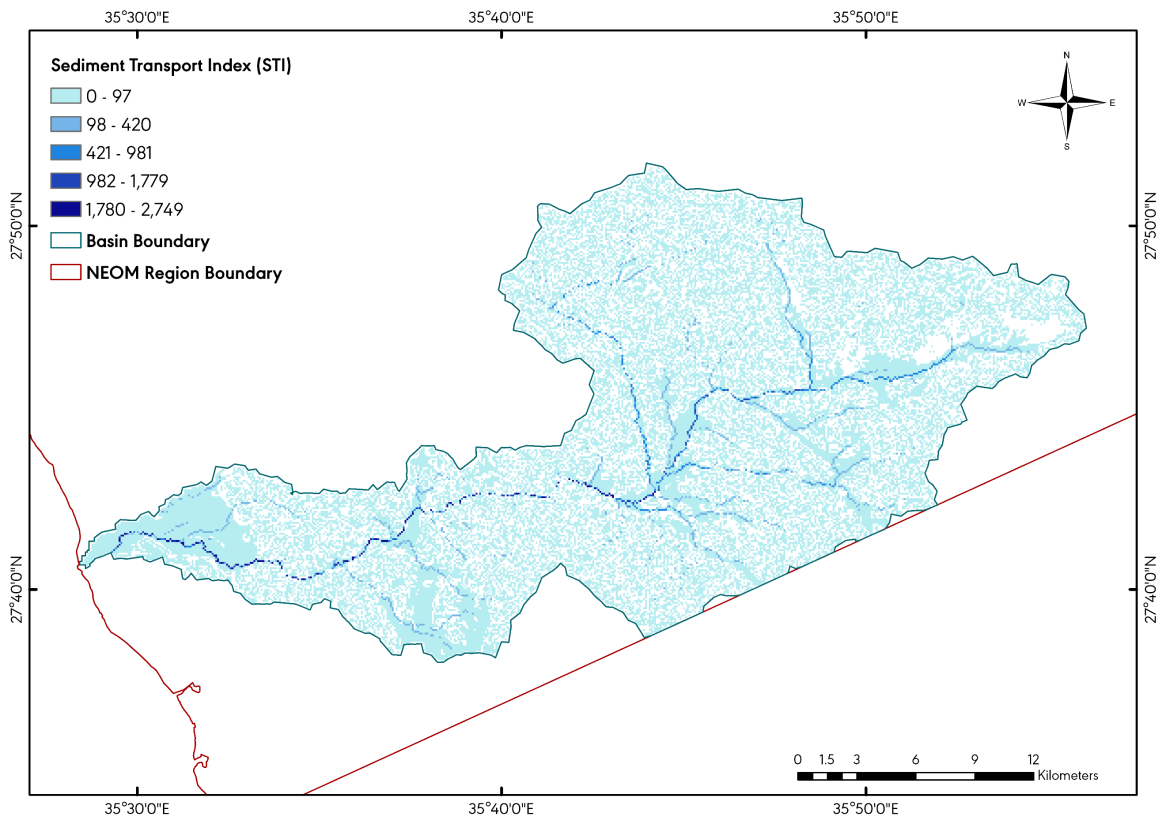
(d)



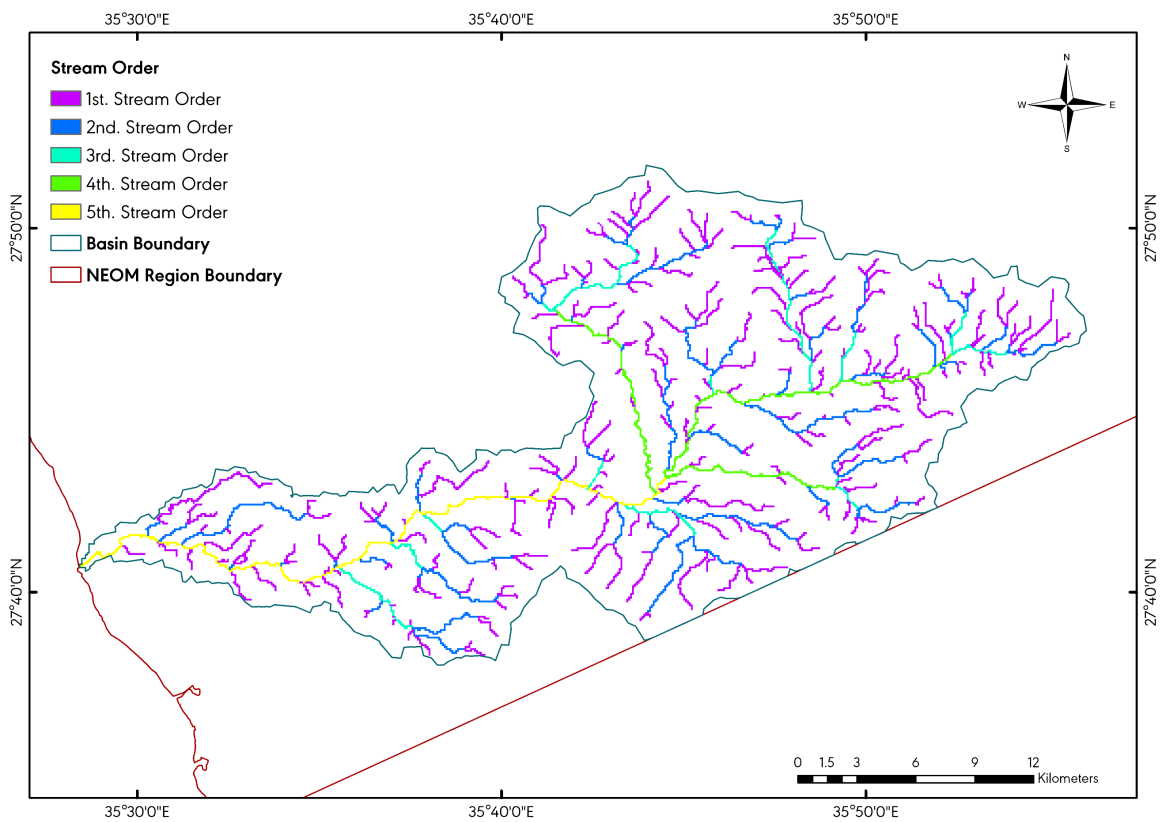
(e)



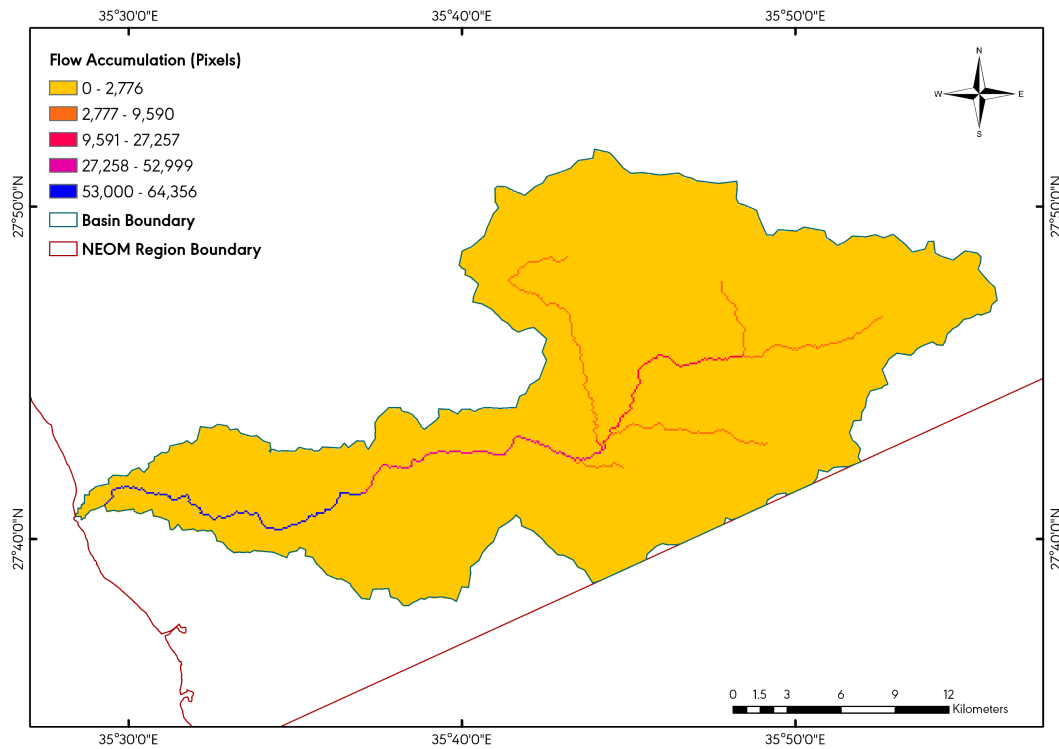
(f)



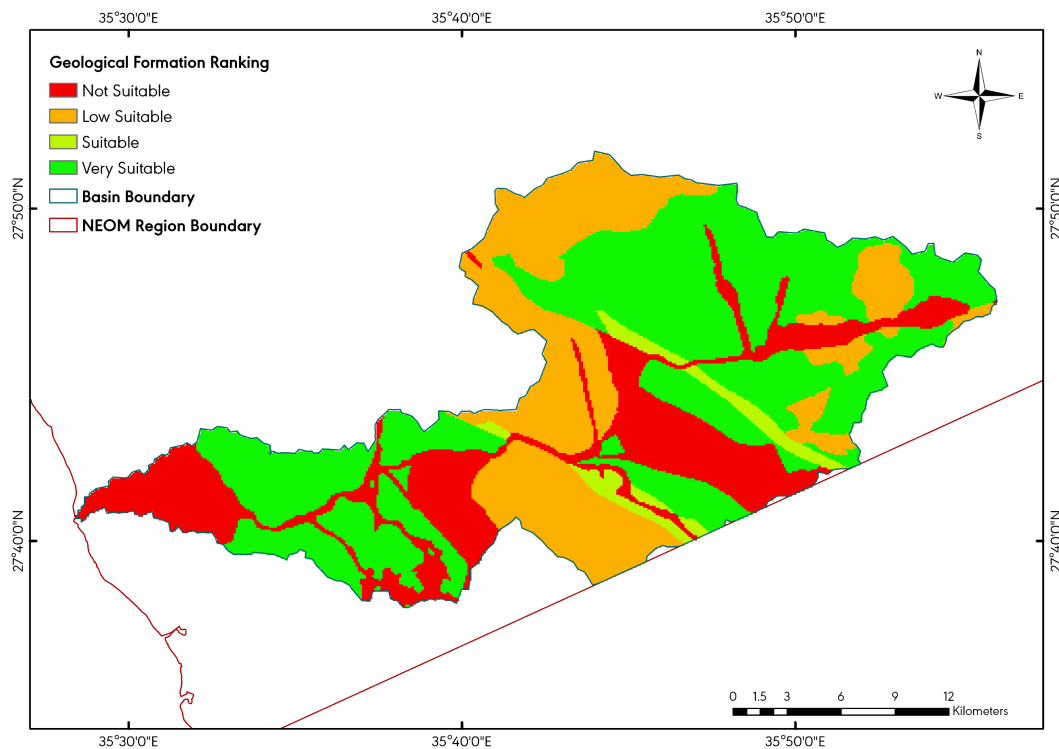
(g)



(h)



(i)



(j)

**Figure 11.** Influencing ten Wadi Surr flash flood causative criteria, including (a) Topographic Wetness Index (TWI), (b) Elevation, (c) Slope, (d) Stream Power Index (SPI), (e) Topographic Roughness Index (TRI), (f) Normalized Difference Vegetation Index (NDVI), (g) Sediment Transport Index (STI), (h) Stream Order, (i) Flow Accumulation, and (j) Geological Formation Ranking.

**Table 5.** Susceptibility class score of each causative criteria.

Flash Floods Causative Criteria	Wadi Surr			Wadi Zawhi			Weight (%)
	Class	Susceptibility Class Ranges and Ratings	Susceptibility Class Score	Class	Susceptibility Class Ranges and Ratings	Susceptibility Class Score	
<b>Topographic Wetness Index (TWI)</b>	-7.49 - -4.91	Very Low	1	-7.37 - -4.76	Very Low	1	<b>4</b>
	-4.9 - -2.95	Low	2	-4.75 - -2.95	Low	2	
	-2.94 - -0.37	Moderate	3	-2.94 - -0.56	Moderate	3	
	-0.36 - 3.25	High	4	-0.55 - 2.84	High	4	
	3.26 - 18.84	Very High	5	2.85 - 11.08	Very High	5	
<b>Elevation (Meters)</b>	0 - 291	Very High	5	-2 - 269	Very High	5	<b>9</b>
	292 - 542	High	4	270 - 565	High	4	
	543 - 851	Moderate	3	566 - 961	Moderate	3	
	852 - 1280	Low	2	962 - 1402	Low	2	
	1281 - 2291	Very Low	1	1403 - 2211	Very Low	1	
<b>Slope (Degree)</b>	0 - 6.25	Very High	5	0 - 4.9	Very High	5	<b>15</b>
	6.26 - 13.85	High	4	4.91 - 12.47	High	4	
	13.86 - 21.67	Moderate	3	12.48 - 22.93	Moderate	3	
	21.68 - 30.15	Low	2	22.94 - 34.51	Low	2	
	30.16 - 56.96	Very Low	1	34.52 - 56.78	Very Low	1	
<b>Stream Power Index (SPI)</b>	0 - 0.5	Very Low	1	0 - 0.1	Very Low	1	<b>13</b>
	0.51 - 2.06	Low	2	0.11 - 0.36	Low	2	
	2.07 - 4.45	Moderate	3	0.37 - 0.76	Moderate	3	
	4.46 - 8.89	High	4	0.77 - 1.34	High	4	
	8.9 - 14.17	Very High	5	1.35 - 2.47	Very High	5	
<b>Terrain Roughness Index (TRI)</b>	0.11 - 0.34	Very Low	1	0.11 - 0.31	Very Low	1	<b>3</b>
	0.35 - 0.42	Low	2	0.32 - 0.41	Low	2	
	0.43 - 0.49	Moderate	3	0.42 - 0.48	Moderate	3	
	0.5 - 0.57	High	4	0.49 - 0.56	High	4	
	0.58 - 0.83	Very High	5	0.57 - 0.8	Very High	5	
<b>Normalized Difference Vegetation Index (NDVI)</b>	-0.06 - 0.01	Very High	5	-0.07 - -0.01	Very High	5	<b>7</b>
	0.02 - 0.03	High	4	0 - 0.02	High	4	
	0.04 - 0.06	Moderate	3	0.03 - 0.04	Moderate	3	
	0.07 - 0.1	Low	2	0.05 - 0.06	Low	2	
	0.11 - 0.31	Very Low	1	0.07 - 0.14	Very Low	1	

## Continued

<b>Sediment Transport Index (STI)</b>	0 - 97	Very Low	1	0 - 73	Very Low	1	<b>3</b>
	98 - 420	Low	2	74 - 277	Low	2	
	421 - 992	Moderate	3	278 - 673	Moderate	3	
	993 - 1789	High	4	674 - 1201	High	4	
	1790 - 2749	Very High	5	1202 - 1683	Very High	5	
<b>Stream Order</b>	1 <sup>st</sup>	Very Low	1	1 <sup>st</sup>	Very Low	1	<b>23</b>
	2 <sup>nd</sup>	Low	2	2 <sup>nd</sup>	Low	2	
	3 <sup>rd</sup>	Moderate	3	3 <sup>rd</sup>	Moderate	3	
	4 <sup>th</sup>	High	4	4 <sup>th</sup>	High	4	
	5 <sup>th</sup>	Very High	5	5 <sup>th</sup>	Very High	5	
<b>Flow Accumulation (Pixels)</b>	0 - 2776	Very Low	1	0 - 1370	Very Low	1	<b>13</b>
	2777 - 9590	Low	2	1371 - 5022	Low	2	
	9591 - 27,257	Moderate	3	5023 - 12,897	Moderate	3	
	27,258 - 52,999	High	4	12,898 - 18,831	High	4	
	53,000 - 64,356	Very High	5	18,832 - 29,103	Very High	5	
<b>Geological Formation</b>	Quaternary Sand, Gravel, and Silt Deposits	Not Suitable	1	Quaternary Sand, Gravel, and Silt Deposits	Not Suitable	1	<b>10</b>
	Atiyah Monzogranite, Alkali-Feldspar Granite	Less Suitable	2	Marabat Suite, Atiyah Monzogranite	Less Suitable	2	
	Conglomerate, Siltstone and Silicic Volcaniclastic Rocks	Moderate	3	Alkali-Feldspar Granite	Moderate	3	
	Andesitic lavas, Porphyritic Amphibolite and Pyroclastic Rocks	Suitable	4	Pyroclastic Rocks	Suitable	4	
				Igneous Intrusive Rocks	High Suitable	5	
<b>Total</b>						<b>100</b>	

flash flood hazard. As illustrated in **Figure 12** and **Figure 13**, a flash flood susceptibility map reveals that 9.16% of Wadi Surr channel runoff is sensitive to a very high risk of flooding, 50.13 % is vulnerable to a high risk, 40.36% is vulnerable to a low risk, and 0.35% is vulnerable to a very low risk. Flooding threatens 0.23 percent of the Wadi Zawhi region, 14.33 percent is high risk, 50.99% is medium, 34.27% is low, and 0.18% is extremely low. They are particularly prevalent in the western edge of the Wadi Surr basin and the southwest side of the Wadi Zawhi basin.

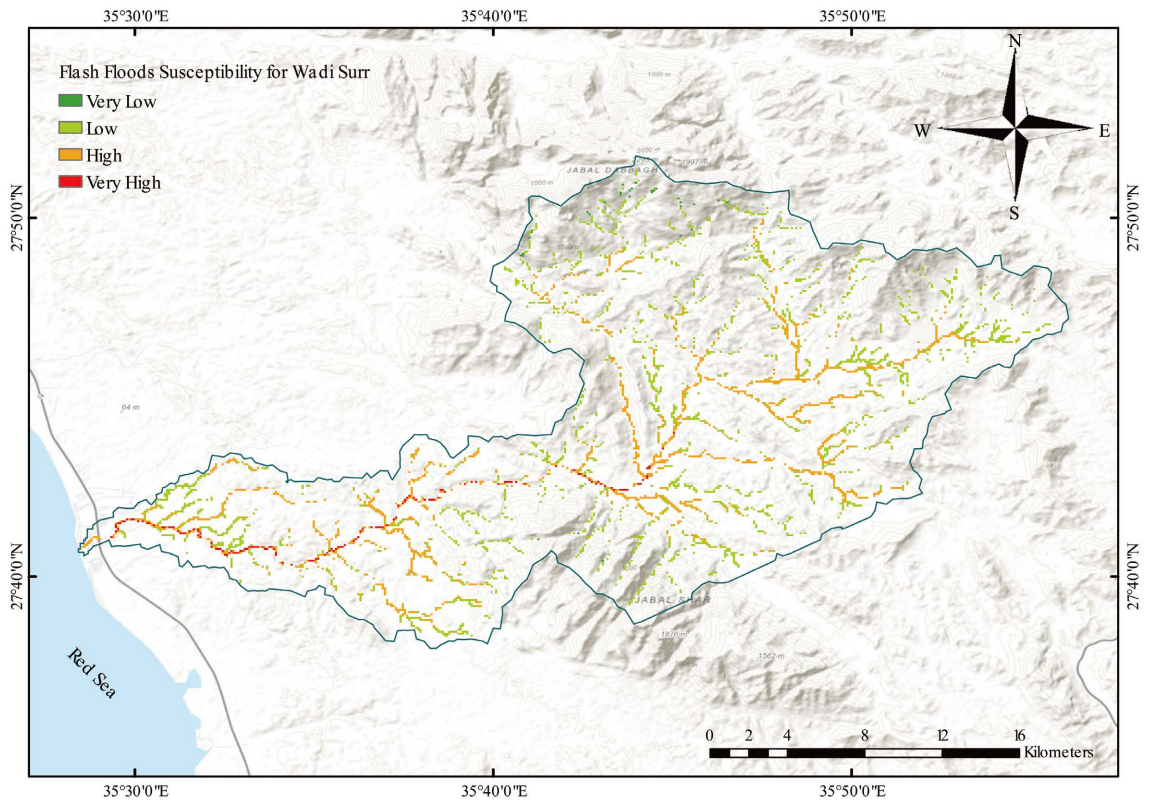


Figure 12. Flood susceptibility map of Wadi Surr derived by the analytic hierarchy process method.

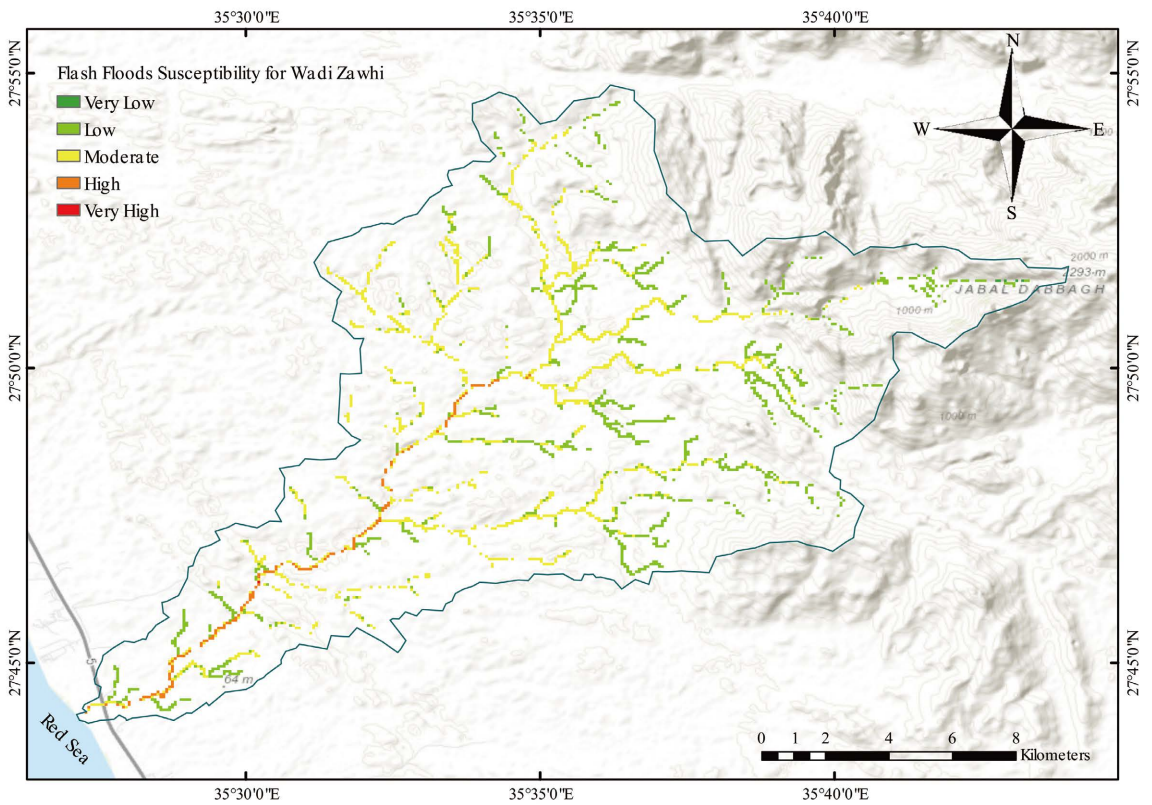


Figure 13. Flood susceptibility map of Wadi Zawhi derived by the analytic hierarchy process method.

## 5. Conclusion

This study aimed to construct flood susceptibility zones for the NEOM region watersheds using Multi-Criteria Decision Analysis (MCDA), precisely the AHP technique, remote sensing, and Geographic Information Systems (GIS). Ten flash flood conditioning criteria were developed to assess where hazardous flash floods are most likely to occur. Each flood conditioning factor was represented by a raster dataset developed in GIS. The AHP was used to create the factor weights depending on the information provided. The approach used in this study has the potential to be used to generate recommendations for flood management in the study region based on the findings. Furthermore, the methodology used in this study can be successfully applied to other studies conducted in other parts of the world, using the same or similar data as that used in this study.

## 6. Recommendations

For the most vulnerable areas of the NEOM region against flooding:

1) Water defense infrastructure is required, including natural defenses like dunes and artificial defenses like dikes, dams, and storm surge barriers. Sensors activate when the water level in the surrounding area rises, closing the barrier's walls and filling its water tanks. The walls are pressed firmly against their bases by the water pressure, preventing floodwaters from breaching the gates. Large swaths of the NEOM region would be flooded if these defenses were not in place. Minor engineering procedures include terraced farm crops, stone walls on a bank, and the development of forested lands and pastures (stabilizing small stream beds with stone thresholds, strengthening steep slopes, and stabilizing drainage ditches). By limiting the effects of increased runoff from urbanization, non-structural techniques such as spatial planning can help reduce hazards in a flash flood-prone catchment. Storms can cause violent shifts or develop, resulting in significantly higher water levels, posing a significant flood risk to coastal areas and communities near large lakes.

2) Flood susceptibility mapping is helpful for planning flood disasters and emergency flood response. Estimating flood susceptibility areas should be a top priority for policymakers, as it is crucial for national and local governments in flood-prone areas.

3) Additionally, existing drainage and sewerage systems must be upgraded, and new high-quality rain drainage systems must be installed, particularly in relatively flat areas.

4) The study recommends updating and accurate spatial geodatabases in hydrology, meteorology, topography, geology, and morphometry.

## Acknowledgements

This paper is dedicated to my mother, Aisha A. Sha'ar (1951-2022), who passed away not long ago and is responsible for shaping who I am today. I would never have been able to finish my master's degree if she hadn't shown me love and

support on a consistent basis all the way through the procedure. In order for you, mother, to understand how much I admire you and how much appreciation I have for everything you've done for me, I would like to demonstrate my gratitude in some way. May Allah bless your soul, mother.

In addition, this job could not have been achieved without the assistance of other people. My primary instructor, Dr. Tarek A. El Damaty, was always available whenever I required direction, support, or assistance. Now, it is my opportunity to thank him. His patience with me will be remembered forever. Without him, I could not have achieved success.

### Conflicts of Interest

The authors declare no conflicts of interest regarding the publication of this paper.

### References

- [1] Al Saud, M.M. (2020) Sustainable Land Management for NEOM Region. Springer, Berlin, 220. <https://doi.org/10.1007/978-3-030-57631-8>
- [2] Youssef, A.M., Pradhan, B. and Sefry, S.A. (2016) Flash Flood Susceptibility Assessment in Jeddah City (Kingdom of Saudi Arabia) Using Bivariate and Multivariate Statistical Models. *Environmental Earth Sciences*, **75**, 1-16. <https://doi.org/10.1007/s12665-015-4830-8>
- [3] Alfawzan, F., Alleman, J.E. and Rehmann, C.R. (2020) Wind Energy Assessment for Neom City, Saudi Arabia. *Energy Science & Engineering*, **8**, 755-767. <https://doi.org/10.1002/ese3.548>
- [4] Kahal, A.Y., Abdelrahman, K., Alfaifi, H.J. and Yahya, M.M. (2021) Landslide Hazard Assessment of the Neom Promising City, Northwestern Saudi Arabia: An Integrated Approach. *Journal of King Saud University—Science*, **33**, Article ID: 101279. <https://doi.org/10.1016/j.jksus.2020.101279>
- [5] Awan, A.B. (2019) Performance Analysis and Optimization of a Hybrid Renewable Energy System for Sustainable Neom City in Saudi Arabia. *Journal of Renewable and Sustainable Energy*, **11**, Article ID: 025905. <https://doi.org/10.1063/1.5071449>
- [6] Dasari, H.P., Desamsetti, S., Langodan, S., Karumuri, R.K., Singh, S. and Hoteit, I. (2020) Atmospheric Conditions and Air Quality Assessment over NEOM, Kingdom of Saudi Arabia. *Atmospheric Environment*, **230**, Article ID: 117489. <https://doi.org/10.1016/j.atmosenv.2020.117489>
- [7] Rezk, H., Alghassab, M. and Ziedan, H.A. (2020) An Optimal Sizing of Stand-Alone Hybrid PV-Fuel Cell-Battery to Desalinate Seawater at Saudi Neom City. *Processes*, **8**, Article No. 382. <https://doi.org/10.3390/pr8040382>
- [8] Niyazi, B., Zaidi, S. and Masoud, M. (2019) Comparative Study of Different Types of Digital Elevation Models on the Basis of Drainage Morphometric Parameters (Case Study of Wadi Fatimah Basin, KSA). *Earth Systems and Environment*, **3**, 539-550. <https://doi.org/10.1007/s41748-019-00111-2>
- [9] Waikar, M.L. and Nilawar, A.P. (2014) Morphometric Analysis of a Drainage Basin Using Geographical Information System: A Case Study. *International Journal of Multidisciplinary and Current Research*, **2**, 179-184.
- [10] Miller, V.C. (1953) A Quantitative Geomorphic Study of Drainage Basin Characteristics in the Clinch Mountain Area Virginia and Tennessee. Columbia University,

New York.

- [11] Gregory, K.J. and Walling, D.E. (1973) Drainage Basin Form and Process.
- [12] Strahler, A.N. (1964) Quantitative Geomorphology of Drainage Basin and Channel Networks. In: Chow, V., Ed., *Handbook of Applied Hydrology*, McGraw Hill, New York, 439-476.
- [13] DaVis, J.C. (1975) Statics and Data Analysis in Geology.
- [14] Acharya, T.D. and Yang, I. (2015) Exploring Landsat 8. *International Journal of IT, Engineering and Applied Sciences Research (IJIEASR)*, **4**, 4-10.
- [15] Schumm, S.A. (1956) Evolution of Drainage Systems and Slopes in Badlands at Perth Amboy, New Jersey. *Geological Society of America Bulletin*, **67**, 597-646. [https://doi.org/10.1130/0016-7606\(1956\)67\[597:EODSAS\]2.0.CO;2](https://doi.org/10.1130/0016-7606(1956)67[597:EODSAS]2.0.CO;2)
- [16] Horton, R.E. (1945) Erosional Development of Streams and Their Drainage Density: Hydrophysical Approach to Quantitative Geomorphology. *Geological Society of America Bulletin*, **56**, 275-370. [https://doi.org/10.1130/0016-7606\(1945\)56\[275:EDOSAT\]2.0.CO;2](https://doi.org/10.1130/0016-7606(1945)56[275:EDOSAT]2.0.CO;2)
- [17] Smith, K.G. (1950) Standards for Grading Texture of Erosional Topography. *American Journal of Science*, **248**, 655-668. <https://doi.org/10.2475/ajs.248.9.655>
- [18] Horton, R.E. (1932) Drainage-Basin Characteristics. *Transactions, American Geophysical Union*, **13**, 350-361. <https://doi.org/10.1029/TR013i001p00350>
- [19] Haggett, P. (1966) Locational Analysis in Human Geography.
- [20] Faniran, A. (1968) The Index of Drainage Intensity: A Provisional New Drainage Factor. *Australian Journal of Science*, **31**, 326-330.
- [21] Melton, M.A. (1957) Geometric Properties of Mature Drainage Basin Systems and Their Representation in Their E4 Phase Space. *The Journal of Geology*, **66**, 35-56. <https://doi.org/10.1086/626481>
- [22] Sreedevi, P.D., Subrahmanyam, K. and Ahmed, S. (2004) The Significance of Morphometric Analysis for Obtaining Groundwater Potential Zones in a Structurally Controlled Terrain. *Environmental Geology*, **47**, 412-420. <https://doi.org/10.1007/s00254-004-1166-1>
- [23] Melton, M.A. (1965) The Geomorphic and Paleoclimatic Significance of Alluvial Deposits in Southern Arizona. *The Journal of Geology*, **73**, 1-38. <https://doi.org/10.1086/627044>
- [24] Chorley, R.J. and Morley, L.S.D. (1959) A Simplified Approximation for the Hypsometric Integral. *The Journal of Geology*, **67**, 566-571. <https://doi.org/10.1086/626608>
- [25] Singh, P., Gupta, A. and Singh, M. (2014) Hydrological Inferences from Watershed Analysis for Water Resource Management Using Remote Sensing and GIS Techniques. *The Egyptian Journal of Remote Sensing and Space Science*, **17**, 111-121. <https://doi.org/10.1016/j.ejrs.2014.09.003>
- [26] Beven, K.J. and Kirkby, M.J. (1979) A Physically Based, Variable Contributing Area Model of Basin Hydrology/Un modèle à base physique de zone d'appel variable de l'hydrologie du bassin versant. *Hydrological Sciences Journal*, **24**, 43-69. <https://doi.org/10.1080/02626667909491834>
- [27] Sørensen, R. and Seibert, J. (2007) Effects of DEM Resolution on the Calculation of Topographical Indices: TWI and Its Components. *Journal of Hydrology*, **347**, 79-89. <https://doi.org/10.1016/j.jhydrol.2007.09.001>
- [28] Sarker, M.Z. and Sivertun, Å. (2011) GIS and RS Combined Analysis for Flood Prediction Mapping—A Case Study of Dhaka City Corporation, Bangladesh. *Interna-*

- tional Journal of Environmental Protection*, **1**, 30-42.  
<https://doi.org/10.5963/IJEP0103005>
- [29] Jozaghi, A., Alizadeh, B., Hatami, M., Flood, I., Khorrami, M., Khodaei, N. and Ghasemi Tousi, E. (2018) A Comparative Study of the AHP and TOPSIS Techniques for Dam Site Selection Using GIS: A Case Study of Sistan and Baluchestan Province, Iran. *Geosciences*, **8**, Article No. 494.  
<https://doi.org/10.3390/geosciences8120494>
- [30] Wu, Y., Zhong, P.A., Zhang, Y., Xu, B., Ma, B. and Yan, K. (2015) Integrated Flood Risk Assessment and Zonation Method: A Case Study in Huaihe River Basin, China. *Natural Hazards*, **78**, 635-651. <https://doi.org/10.1007/s11069-015-1737-3>
- [31] Pei, T., Qin, C.Z., Zhu, A.X., Yang, L., Luo, M., Li, B. and Zhou, C. (2010) Mapping Soil Organic Matter Using the Topographic Wetness Index: A Comparative Study Based on Different Flow-Direction Algorithms and Kriging Methods. *Ecological Indicators*, **10**, 610-619. <https://doi.org/10.1016/j.ecolind.2009.10.005>
- [32] Burrough, P.A., McDonnell, R.A. and Lloyd, C.D. (2015) Principles of Geographical Information Systems. Oxford University Press, Oxford.
- [33] Mojaddadi, H., Pradhan, B., Nampak, H., Ahmad, N. and Ghazali, A.H.B. (2017) Ensemble Machine-Learning-Based Geospatial Approach for Flood Risk Assessment Using Multi-Sensor Remote-Sensing Data and GIS. *Geomatics, Natural Hazards and Risk*, **8**, 1080-1102. <https://doi.org/10.1080/19475705.2017.1294113>
- [34] Nellemann, C. and Reynolds, P.E. (1997) Predicting Late Winter Distribution of Muskoxen Using an Index of Terrain Ruggedness. *Arctic and Alpine Research*, **29**, 334-338. <https://doi.org/10.2307/1552148>
- [35] Khosravi, K., Pourghasemi, H.R., Chapi, K. and Bahri, M. (2016) Flash Flood Susceptibility Analysis and Its Mapping Using Different Bivariate Models in Iran: A Comparison between Shannon's Entropy, Statistical Index, and Weighting Factor Models. *Environmental Monitoring and Assessment*, **188**, Article No. 656.  
<https://doi.org/10.1007/s10661-016-5665-9>
- [36] Khosravi, K., Nohani, E., Maroufinia, E. and Pourghasemi, H.R. (2016) A GIS-Based Flood Susceptibility Assessment and Its Mapping in Iran: A Comparison between Frequency Ratio and Weights-of-Evidence Bivariate Statistical Models with Multi-Criteria Decision-Making Technique. *Natural Hazards*, **83**, 947-987.  
<https://doi.org/10.1007/s11069-016-2357-2>
- [37] Moore, I.D. and Wilson, J.P. (1992) Length-Slope Factors for the Revised Universal Soil Loss Equation: Simplified Method of Estimation. *Journal of Soil and Water Conservation*, **47**, 423-428.
- [38] Kalantari, Z., Nickman, A., Lyon, S.W., Olofsson, B. and Folkesson, L. (2014) A Method for Mapping Flood Hazard along Roads. *Journal of Environmental Management*, **133**, 69-77. <https://doi.org/10.1016/j.jenvman.2013.11.032>
- [39] Saaty, T.L. (1980) The Analytic Hierarchy Process. McGraw-Hill, New York, 324.  
<https://doi.org/10.21236/ADA214804>